Journal of Non-Crystalline Solids 612 (2023) 122351

Contents lists available at ScienceDirect

Journal of Non-Crystalline Solids

journal homepage: www.elsevier.com/locate/jnoncrysol

Review

Glasses and glass-ceramics in the CaO–MgO–SiO_2 system: Diopside containing compositions - A brief review

Dilshat U. Tulyaganov [a], Konstantinos Dimitriadis [b], Simeon Agathopoulos [c], Hugo R. Fernandes [d,*]

[a] Turin Polytechnic University in Tashkent, 17 Small Ring Street, Tashkent 100095, Uzbekistan
[b] Division of Dental Technology, Department of Biomedical Sciences, University of West Attica, Athens, Greece
[c] Department of Materials Science and Engineering, University of Ioannina, Ioannina 451 10, Greece
[d] Department of Materials and Ceramic Engineering, CICECO, University of Aveiro, Aveiro 3810-193, Portugal

ARTICLE INFO

Keywords:
Phase diagram
CaO−MgO−SiO_2 system
Glasses
Glass-ceramics
Application

ABSTRACT

Among different silicate systems, CaO−MgO−SiO_2 is the one of the most promising due to abundance of reagents, easier fabrication, improved performance, and wide range of application. Analysis of the current literature sources denotes that phase diagram of CaO−MgO−SiO_2 system is regularly used by researchers worldwide as constitutive model for synthesis glass-ceramic materials (GCs) possessing an adequate combination of high chemical durability, mechanical and electrical properties. In recent years, materials from this system attracted extra interest for applications in bone tissue repair owing to their ability to induce hydroxyapatite formation in contact with body fluids and to be resorbed in controllable degradation rate.

In this brief review diopside containing compositions are specifically discussed. The main goal is to provide critical analysis of the experimental trials directed on synthesis of GC materials in the CaO−MgO−SiO_2 system. Glass compositions were analysed through the standpoint of their location in the relevant region, or phase field, within a phase diagram to guide GC production and to make educated choices of compositions and processing parameters.

Apart from Introduction and Conclusions this review comprises five consecutive parts. In the first part, constitution of phase diagram of CaO−MgO−SiO_2 system is comprehensively discussed with connection to melts' crystallization path and crystalline phase formation. In the second part, special attentiveness is drawn towards diopside- containing GCs produced from wastes and non-expensive natural raw materials. In this regard and taking into consideration presence of Al_2O_3 in the majority types of wastes, cross sections of CaO−MgO−SiO_2−Al_2O_3 system with 10, 15 and 20% of Al_2O_3 are suggested to utilize when anticipating ultimate crystalline phase(s) formation. The following parts of this review are mostly addressed to recent advancement in producing optimized diopside-containing glass–ceramic biomaterials for bone repair as well as innovative sealants for solid oxide fuel cells (SOFC). Likewise, some other active areas of research and application for diopside containing GC compositions are briefly discussed.

1. Introduction

The glass and glass-ceramic materials possess a great practical value and their role becoming increasingly important in modern science, industry and common daily life.

Indeed, glass as an essential material has always been a faithful servant of man and currently adapted itself to present-day requirements in numerous branches of modern technology. It exhibits an exceptional versatility in terms of composition and related properties, thus being suitable for taking part in countless applications in arts as well as advanced science and technology.

Glass-ceramics (GCs) are relatively new materials in the glass industry that have been discovered as the result of research on devitrification - an age-old problem in glassmaking. GCs are polycrystalline composite materials that may contain one or more crystalline phases dispersed in a residual glass matrix. The desired properties can be

* Corresponding author.
E-mail address: h.r.fernandes@ua.pt (H.R. Fernandes).

https://doi.org/10.1016/j.jnoncrysol.2023.122351
Received 21 February 2023; Received in revised form 7 April 2023; Accepted 18 April 2023
Available online 28 April 2023

obtained due to careful attention to the composition of the batch and the controlled crystallization of certain "parent" glasses [1]. Generally, crystallization is considered as consisting of two independent processes: nucleation, which corresponds to the formation of crystal nuclei, and crystal growth from the formed centres. Nucleating agents, which are typically added in amount of a few percent, play a critical role to promote volume nucleation and enables a GCs to be produced [1,2]. The micro- or nanostructures of GCs and the distinct chemical nature of the crystalline phases favours the development of desirable combinations of properties and brand-new applications. Nowadays glasses and GCs remain irreplaceable in many fields of human activity including electronics, optics, architecture, building, energy, waste management, space, defense, healthcare and domestics. In turn, accelerated development of technology, globalization, increased environmental regulation and rising energy costs are the main challenges that currently facing glass/GC industry to its competitiveness. Therefore, careful choice of glass systems and appropriate design a glass-ceramic compositions along with advances in understanding the process of crystallization are among those important instruments that allow to synthesize a final product with near-ideal properties to fulfill the requirements for a particular application [2]. It was observed that simple glasses with composition near the stoichiometry of a crystalline phase and near the position of the eutectics on relevant phase diagrams devitrify copiously with the high-volume fraction of the crystalline phase up to 90%. However, with increase in the number of reagents in glass batch crystallization is a more complex process: metastable crystalline phases commonly precipitate at initial stages of crystallization that transform into the thermodynamically stable phase relevant with the phase diagram of the system on further heating steps [2,3].

The type of crystals precipitated from a glass reservoir can be represented via the time-temperature-transformation diagrams. Concomitantly, considering that phase relations are critical to successful fabrication, the nature of the crystalline phases formed upon heat treatment can be approximately predicted from the relevant system phase diagram [4].

Importantly, that phase diagrams represent thermodynamic equilibrium whereas in normal industrial operating conditions thermodynamic equilibrium is not usually attained. Therefore, it is not surprise that often phases obtained upon devitrification of glasses at a certain heat treatment procedure are not thermodynamically favoured according to the phase diagram but are kinetically determined products [2]. Nevertheless, the equilibrium phase diagram of the relevant system might be helpful in configurating the fields of main phases formed at particular conditions with variations in composition and thus can still be used to predict the tendency of the reaction to complete [2–5].

Among investigated silicate systems the $CaO-MgO-SiO_2$ one is of great importance in metallurgy and geochemistry and is essential for many technical silicate products such as dolomitic refractories, magnesian Portland cements, magnesian ceramic masses, metallurgical slags, glasses and GC materials [6,7]. One of the key advantages of selecting glass/GC composition from $CaO-MgO-SiO_2$ system is the chance to apply for abundant natural rocks and various industrial wastes as initial raw materials for glass batch preparation. Importantly, in the last few decades GC materials based on $CaO-MgO-SiO_2$ system attracted significant attention worldwide due to their excellent bioactive properties [8–10] along with biocompatibility [11], and biodegradation ability [12]. Noteworthy, pyroxene-based glass-ceramic seals have been specifically discussed in the literature because those have achieved appropriate thermal and chemical properties along with high stability [13–16].

The main objective of this work is to provide critical analysis of the experimental trials directed on to synthesis of GC materials in the $CaO-MgO-SiO_2$ system. The composition will be analysed through the standpoint of their location in the phase diagrams to guide glass-ceramic production and to make educated choices of compositions and processing parameters. The special attention is drawn to diopside based glassy materials developed from natural raw materials and wastes, glasses and GCs for application as sealants for solid oxide fuel cells (SOFC) and for biomedical application. The truth is that both glasses produced through the classical melt-quench and sol-gel technique are inevitable parts of this system, but the latter ones lie beyond the scope of this review.

2. The phase diagram of $CaO-MgO-SiO_2$ system

The phase relationships in the $CaO-MgO-SiO_2$ system were first investigated by Ferguson and Merwin [17]. Fig. 1 represents the phase diagram of $CaO-MgO-SiO_2$ system as reported by Osborn and Maun [18] with four established ternary compounds. Monticellite ($CaO{\cdot}MgO{\cdot}SiO_2$) melts incongruently at 1485 °C with decomposition into liquid and periclase MgO. Monticellite features an island structure of the olivine type, similar to the structure of $\gamma-2CaO{\cdot}SiO_2$ and forsterite ($2MgO{\cdot}SiO_2$). It occurs in nature and may appear in the blast-furnace and open-hearth furnace slags. Mervinate ($3CaO{\cdot}MgO{\cdot}2SiO_2$) is a compound that melts incongruently at 1575 °C, decomposing into liquid, $2CaO{\cdot}SiO_2$ and MgO. Mervinate's structure resembles α'-Ca_2SiO_4 so that there was even an assumption that merwinite is one of the forms of α'-Ca_2SiO_4. It is known as a natural mineral and is found in some technical products and, in particular, in various slags, dolomite refractories, etc. Akermanite ($2CaO{\cdot}MgO{\cdot}2SiO_2$) is a compound that melts congruently at 1454 °C, it is found in nature and in some technical products, mainly in blast-furnace slags and some non-ferrous metallurgy slags.

Diopside ($CaO{\cdot}MgO{\cdot}2SiO_2$) melts congruently at 1390 °C. Diopside is built from $[SiO_4]^{4-}$ chains linked by calcium and magnesium ions. Magnesium ions have six-fold coordination and are surrounded by oxygen ions, which belong to different $[SiO_4]^{4-}$ tetrahedra. Calcium ions have an eightfold coordination of oxygen ions, two of which belong to two adjacent $[SiO_4]^{4-}$ tetrahedra. In nature, it is distributed as a mineral of the pyroxene group and forms solid solutions with $MgO{\cdot}SiO_2$ ($MgSiO_3$) due to substitution of Mg^{2+} for Ca^{2+} (despite the significant difference of their ion size of about 40%), hedenbergite ($CaFe_2Si_2O_6$, substitution of Fe for Mg on M1 sites), jadeite ($NaAlSi_2O_6$, substitution of Al for Mg on M1sites and Na for Ca on M2 sites), which play an important role in the constitution of ordinary silicate rock-forming minerals - pyroxenes. The most important clinopyroxene end members in augite are diopside and hedenbergite, while augite ($(Ca,Na)(Mg,Fe,Al,Ti)(Si,Al)_2O_6$) can also accommodate significant aluminum, titanium, sodium and other elements.

The Mohs hardness for diopside is 6 while Vickers hardness is 7.7 GPa at a load of 0.98 N [19], and a specific gravity of 3.25 to 3.55. The diopside ($CaMgSi_2O_6$) glass is usually synthesized by melt-quenching technique in temperature range of 1450–1600 °C [20–24]. Further heat treatment at 1200 °C caused glass transformation to polycrystalline diopside [22].

Diopside glass exhibits tendency towards devitrification as soon as the melt is poured on the metallic mold: spherulitic diopside crystals on the surface of stoichiometric diopside glass as a result of surface nucleation [2]. However, true glass might be produced using faster cooling rates. Thus, Zanotto synthesized diopside glass (with 1 wt% Al_20_3 to minimize spontaneous devitrification) at 1450 °C for 5 h to obtain thin specimens by quenching the molten glass between two steel plates. Surface nucleation occurred very rapidly from some random number of active (impurity) when those specimens were heat treated at 820 °C from 1 to 4 h suggesting heterogeneous crystal nucleation in glass, specifically for nucleation at the glass/air surface [25].

Structural and thermodynamic issues of diopside melt and glass have been thoroughly experimentally investigated and discussed elsewhere [26–32].

The glass transition temperature (T_g) of diopside glass was recorded to be about 985 °C, whilst linear thermal expansion coefficient (CTE) to be $9.12 \times 10^{-6}\ K^{-1}$ [32]. The experimental values of viscosity (η, Poise)

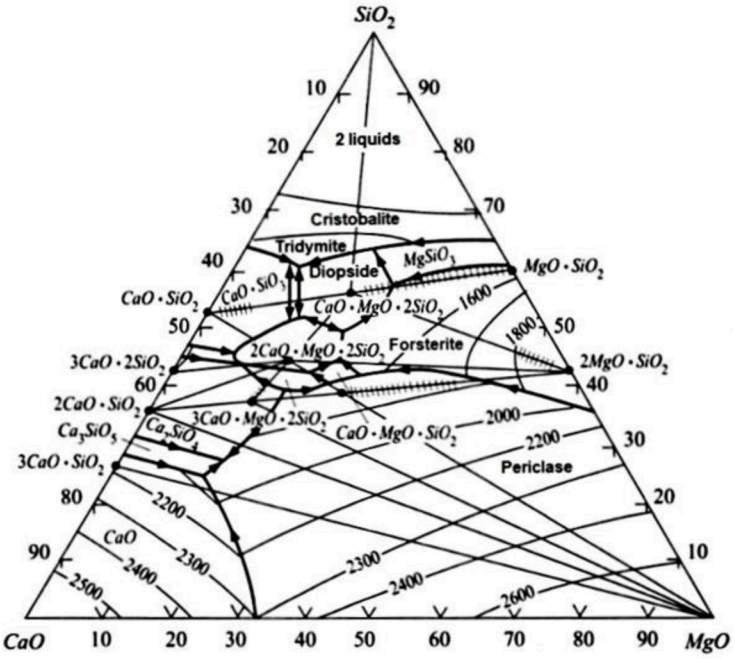

Fig. 1. Phase diagram of CaO−MgO−SiO_2 system as reported by Osborn and Maun [18].

for a stoichiometric diopside glass measured at atmospheric pressure reported to be as follows: $\log \eta = 13.3$ (700 °C), 9.6 (795 °C) [33], 1.086 (1375 °C), 0.678 (1500 °C) and 0.465 (1600 °C) [34], being in good correlation with those reported by Nascimento et al. [20] and Tauber and Arndt [35]. The values of surface tension of diopside melt at 1400 °C, 1500 °C and 1550 °C were found to be 371, 376 and 378 dyne. cm^{-1}, respectively [36,37].

3. Diopside containing glasses and glass ceramics from natural raw materials and wastes

The binary compounds that have their crystallization field in the system are forsterite ($2MgO{\cdot}SiO_2$) and protoenstatite ($MgO{\cdot}SiO_2$, which melts with decomposition), wollastonite ($CaO{\cdot}SiO_2$), tricalcium disilicate ($3CaO{\cdot}2SiO_2$) (melts incongruently), calcium orthosilicate $2CaO{\cdot}SiO_2$ and tricalcium silicate ($3CaO{\cdot}SiO_2$, melts with decomposition). In addition, on the state diagram of the CaO−MgO−SiO_2 system, there are fields of crystallization of periclase MgO, lime CaO and silica SiO_2 in the form of cristobalite and tridymite. Moreover, binary MgO−SiO_2 and CaO−SiO_2 systems have stable glass immiscibility regions, which are merging in silica rich corner of the CaO−MgO−SiO_2 system.

A characteristic feature of the CaO−MgO−SiO_2 system is the formation of solid solutions between many compounds. In the diagram (Fig. 1), they are conventionally indicated by dashes on the connecting lines between the points of the compositions of the compounds that form solid solutions. In particular, monticellite forms a wide (but limited) series of solid solutions with forsterite, and forsterite forms solid solutions with diopside. Limited solid solutions exist between akermanite, on the one hand, and merwinite, rankinite ($3CaO{\cdot}2SiO_2$), forsterite, and calcium orthosilicate, on the other (in the latter case, the solubility is possibly very low). Diopside forms solid solutions with wollastonite ($CaO{\cdot}SiO_2$) and protoenstatite ($MgO{\cdot}SiO_2$). No solid solutions were found between monticellite and merwinite, akermanite and wollastonite, monticellite and calcium orthosilicate.

The most fusible eutectic in the system is formed between wollastonite, diopside and tridymite with a melting point of 1320 °C (Table 1). The diopside crystallization field is limited by two more eutectics with the lowest melting points: one between diopside, akermanite and wollastonite (1350 °C), the second between diopside, akermanite and forsterite (1357 °C). Apparently, the most fusible compositions lie in the diopside crystallization field or in the regions adjacent to it.

Table 1
Some invariant points in the CaO−MgO−SiO_2 system.

№	Equilibrium phases	Process	Composition (wt.%)			Temperature (°C)
			MgO	CaO	SiO_2	
1	$Ca_2MgSi_2O_7$ (akermanite) + $CaSiO_3$ (wollastonite) + $Ca_3MgSi_2O_8$ (mervinite) + liquid	Tributary reaction point	9.2	47.2	43.6	1400
2	$Ca_3MgSi_2O_8$ + $2CaO{\cdot}SiO_2$ + MgO + liquid	Tributary reaction point	21.9	42.6	35.5	1575
3	$Ca_2MgSi_2O_7$ + liquid	Melting	14.7	41.2	44.1	1454
4	$CaMgSiO_4$ (monticellite): MgO + liquid	Incongruent melting				1485
5	$Ca_3MgSi_2O_8$: $2CaO{\cdot}SiO_2$ + MgO + liquid	Incongruent melting				1575
6	$CaMgSiO_6$ (diopside) + liquid	Melting	18.6	25.8	55.6	1390
7	$CaSiO_3$ + SiO_2 + $CaMgSiO_6$ + liquid	Eutectic	8.0	30.6	61.4	1320
8	$CaSiO_3$ + $CaMgSiO_6$ + $Ca_2MgSi_2O_7$ + liquid	Eutectic	12.6	36.0	51.4	1350
9	$CaMgSiO_6$ + $Ca_2MgSi_2O_7$ + Mg_2SiO_4 (forsterite) + liquid	Eutectic	20.2	29.8	50.0	1357

The crystallization paths of melts in a system are often complex due to the fact that the system contains many incongruently melting

compounds and, consequently, incongruent boundary curves. Let us consider some of the crystallization pathways related to the most low-melting compositions of the system, which are important for the technology of pyroxene GCs.

Suppose a composition is located in the crystallization field of diopside and belongs to the elementary phase triangle SiO_2-diopside-wollastonite. This means that the end point of melt solidification will be the eutectic between these three compounds with a melting point of 1320 °C. The primary crystalline phase is diopside. The path of crystallization will go along a straight line connecting the points corresponding to stoichiometric diopside and the initial composition, then along the boundary curve between the fields of crystallization of diopside and tridymite. However, it should be considered that the compositions located near the region of stable segregation, when cooled, can fall into the region of metastable segregation, which serves as a continuation of the dome of stable segregation. Therefore, when the melt of this particular composition is cooled down, metastable segregation is likely to happen and only after that diopside crystals may precipitate.

If the composition is located to the right of the SiO_2-diopside connecting straight line and falls into the SiO_2-diopside-protoenstatite phase triangle, then in this case the end point of the melt solidification will be the point, in which the three phases are in equilibrium with the liquid at a temperature of 1375 °C. However, a further crystallization process of the composition will be affected by metastable segregation and formation of solid solutions – pyroxenes. Therefore, in the final products of crystallization diopside and protoenstatite are not found in pure form while in the form of clinopyroxene solid solutions.

For composition laying in the forsterite-diopside-protoenstatite phase triangle the primary crystalline phase is forsterite. The crystallization path follows the straight-line connecting points corresponding to stoichiometric forsterite and initial composition. When the composition of the melt reaches the boundary curve between the fields of crystallization of forsterite and protoenstatite, a second crystalline phase, $MgO{\cdot}SiO_2$ should appear due to the dissolution of previously separated forsterite, since the boundary curve is incongruent. However, due to the fact that calcium oxide is also present in the melt, in addition to magnesium oxide, it is involved in the emerging crystalline phase. Thus, in this case also pyroxenes are formed. Crystallization ends at the tributary reaction point with a temperature of 1390 °C, since the starting point of composition lies in the forsterite-diopside-protoenstatite phase triangle.

To give an example [38], glass compositions containing SiO_2, CaO, MgO, and Na_2O were examined aiming at achieving bulk crystallization after heat treatment at 670−690 °C and 920–940 °C in the presence of nucleating agents such as CaF_2 and MoO_3 (*e.g.*, in absence of nucleating agents pyroxene based systems are generally prone to surface crystallization owning to the difference between the density of crystals and glassy phase formed). All the experimental glasses (Table 2) are located in the primary crystallization field of cristobalite in the phase diagram of CaO−MgO−SiO_2 system (Fig. 1). Furthermore, the first 3 compositions (*i.e.*, 3, 4 and 5) belong to elementary phase triangle SiO_2-diopside-wollastonite. Therefore, one can anticipate that the end point of melt solidification is ternary eutectic at 1320 °C comprising in equilibrium three crystalline phases and a liquid. Indeed, diopside, wollastonite and cristobalite were revealed while MgO for CaO substitution led to increase in diopside amount at the expense of wollastonite. In the other heat-treated experimental glass compositions (*e.g.*, 6 and 7) that falls into the SiO_2-diopside-protoenstatite phase triangle, XRD analysis confirmed presence of diopside and cristobalite (Table 2).

Five glasses with chemical composition (wt.%) 52.5 − 53.6 SiO_2, 28.1 − 37.0 CaO, 8.8-16.6 MgO, and 4.7 − 4.8 Na_2O were investigated aiming at obtaining wall-covering glass-ceramics [39]. All glasses belong to the elementary phase triangle diopside-wollastonite-akermanite and theoretically the end point of melt solidification is ternary eutectic at 1357 °C comprising in equilibrium three crystalline phases and a liquid. According to the results obtained heat treatment of glasses at 1000 °C for 2 h resulted in formation diopside-wollastonite GCs.

Diopside-containing GCs have been produced from the various resources including wastes [40–50]. Considering presence of Al_2O_3 in the many types of wastes cross sections of CaO−MgO−SiO_2−Al_2O_3 system with 10, 15, 20 and 25 wt.% of Al_2O_3 are more appropriate to apply instead of CaO−MgO−SiO_2 to anticipate formation of crystalline phases (Fig. 2). Table 3 provides information about diopside-containing GCs produced from the industrial wastes such as blast furnace slag and fly ash where certain conventions were applied to anticipate approximate indication of glass composition on the liquids surface of the corresponding phase diagrams. In particular, MgO and Fe_2O_3 contents were integrated (assuming possibility of Fe for Mg on M1 sites in pyroxenes) and then the content of the major constituents was recalculated to set 100% at the expense of the rest components.

Notably, that among other wastes blast furnace slag was the one of the first to be suggested as a valuable source for glass making [40,41]. Actually, this type of slag is the by-product of steel manufacturing industry that occurs in a glassy state and composed mainly of CaO, SiO_2, MgO, and Al_2O_3. Steel industry in China produces about 200 billion tons of blast furnace slag every year [45]. For several decades it was used in production of high lime, low alkali GCs namely “slagsitall” with FeS, MnS and other sulfides served as nucleating agents and wollastonite and diopside precipitated as the primary crystalline phases. Owing to high chemical resistance, refractory properties, high hardness, good to excellent wear resistance and low cost, “slagsitall” materials have been widely used for flooring and for exterior and interior cladding in construction, chemical and petrochemical industries [41,43,44].

The batch of the other extensively studied blast furnace slag based GCs “silceram” [43] was formulated by mixing the slag with up to 30 wt. % colliery shale and other components conferring the following chemical composition (in wt.%): 48.3 SiO_2, 13.3 Al_2O_3, 0.8 Cr_2O_3, 4.0 Fe_2O_3, 0.4 MnO, 5.7 MgO, 24.7 CaO, 1.2 Na_2O, 1.1 K_2O, 0.6 TiO_2. The major constituents of “silceram” are 4 oxides: SiO_2, CaO, MgO and Al_2O_3, and its chemical composition falls into primary crystallization field of pyroxene in the CaO−MgO−SiO_2–Al_2O_3 (15%) system, nearby pyroxene-anorthite boundary (Fig. 2) that theoretically confer precipitation of pyroxene as the principal and anorthite as the minor phases. In the comprehensive review titled “Glass-ceramics: Their production from wastes - A Review”, Rawlingst et al. [43] documented that the main crystalline phase in “silceram” is a pyroxene composition close to diopside with small amount of anorthite (*e.g.*, anorthite may emerge

Table 2
Chemical composition (wt.%) of various glasses belonged to CaO−MgO−SiO_2 system and crystalline phases developed after heat treatment [38]. Note that the convention was applied to anticipate approximate indication of glass composition on the liquids surface of the corresponding phase diagrams: the content of major constituents (*i.e.*, SiO_2, CaO, MgO) was recalculated to set 100% at the expense of minor components.

№	SiO_2	CaO	MgO	Na_2O	CaF_2	MoO_3	Crystalline phases formed upon nucleation and crystallization	Position of glass composition in the phase diagram of the CaO−MgO−SiO_2 system
3	59.68	21.23	6.02	5.08	4.00	4.00	wollastonite, diopside, cristobalite	Elementary phase triangle SiO_2-diopside-wollastonite
4	59.68	18.23	9.02	5.08	4.00	4.00		
5	59.68	15.23	12.02	5.08	4.00	4.00		
6	59.68	12.23	15.02	5.08	4.00	4.00	diopside, cristobalite	Elementary phase triangle SiO_2-diopside-protoenstatite
7	59.68	9.23	18.02	5.08	4.00	4.00		

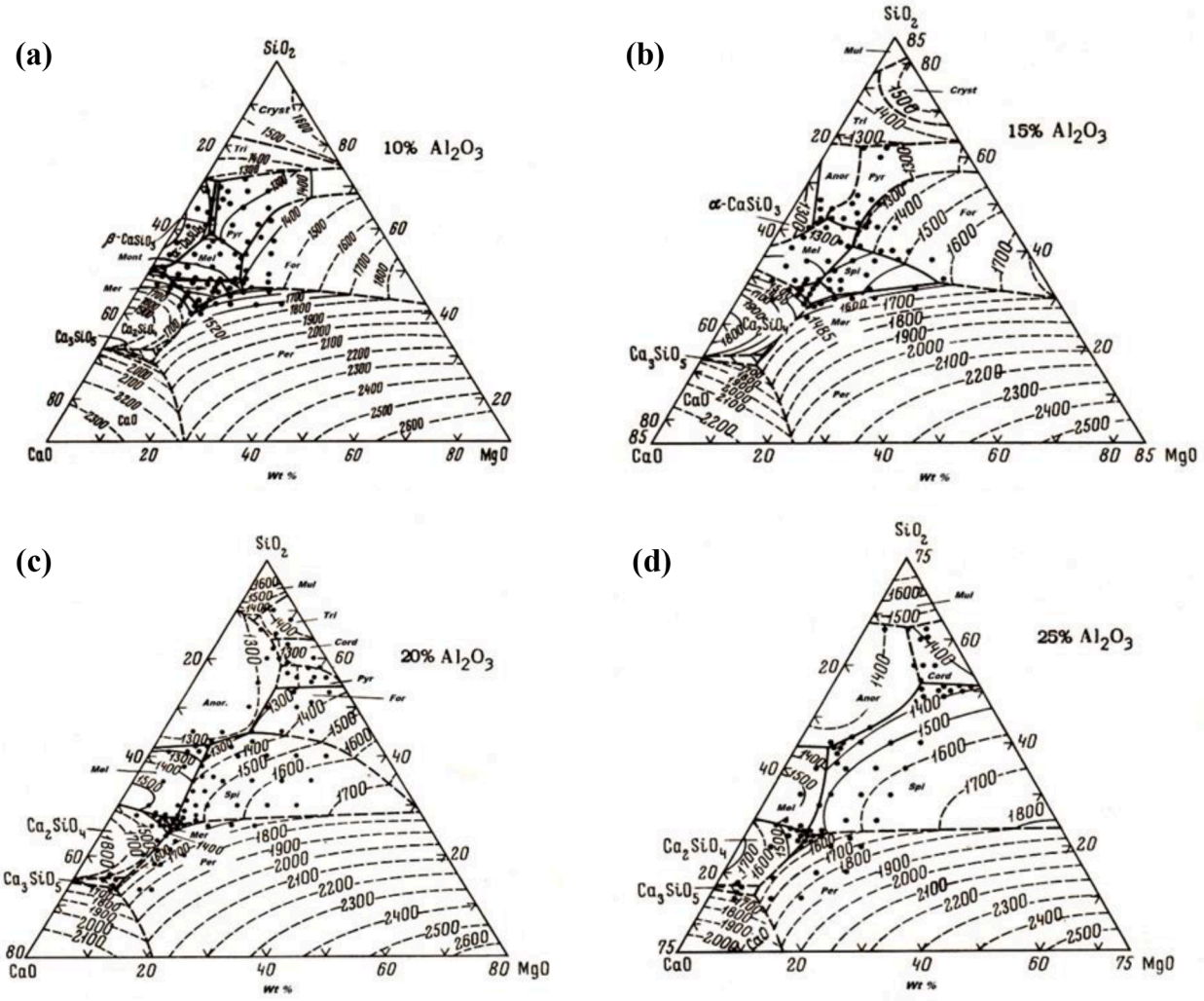

Fig. 2. Liquidus surfaces for cross-sections of CaO–MgO–SiO_2–Al_2O_3 system with (a) 10, (b) 15, (c) 20 and (d) 25 wt.% Al_2O_3 as reported by Osborn et al. [18]: Cryst-cristobalite, Tri-tridymite, Pyr-pyroxene, Anor-anorthite, For-forsterite, Mel-melilite, Mul-mullite, Spi-spinel, Per-periclase, Cord-cordierite.

Table 3
Some compositions of diopside-containing GCs produced from the wastes such as blast furnace slag and fly ash. Note that some conventions were applied to anticipate approximate indication of glass composition on the liquids surface of the corresponding phase diagrams: MgO and Fe_2O_3 were integrated and then the content of the major constituents was recalculated to set 100% at the expense of the rest components.

Type of waste	Parent glass composition, wt.%					Approximate glass composition in the phase diagram		Ref.
	SiO_2	CaO	MgO/ Fe_2O_3	Al_2O_3	The rest	CaO–MgO–SiO_2–Al_2O_3 (10%)	CaO–MgO–SiO_2–Al_2O_3 (15/20%)	
Blast furnace slag used in "silceram" production	48.3	24.7	5.7/4.0	13.3	4.0	–	Primary crystallization field of pyroxene: nearby pyroxene-anorthite boundary (quaternary system with 15% Al_2O_3)	[43]
Blast furnace slag Baowu Iron & Steel - Group A1	48.2	23.9	5.1/0	9.1	13.7	Region nearby melilite-pyroxene boundary	–	[45]
Blast furnace slag Baowu Iron & Steel - Group A2	42.7	23.9	5.1/0	14.5	13.7	–	Region neighbouring pyroxene-melilite boundary (quaternary system with 15% Al_2O_3)	
Fly ash (Spanish carbon fly ash)	48.6	15.7	6.6/6.3	16.9	5.8	–	(a) Primary crystallization field of pyroxene (quaternary system with 15% Al_2O_3) (b) pyroxene-anorthite-forsterite join (quaternary system with 20% Al_2O_3)	[46]
Fly ash (Çayirhan Thermal Power Plant, Turkey)	43.3	16.6	5.9/7.1	13.5	13.5	–	Primary crystallization field of pyroxene (quaternary system with 15% Al_2O_3)	[47]
Fly ashes thermal power stations of Ptolemaida (Greece)	45.5	22.9	13/3.1	11.0	4.5	–	Primary crystallization field of pyroxene, region neighbouring pyroxene-forsterite boundary (quaternary system with 15% Al_2O_3)	[48]

only after excessively long heat treatment). The fracture toughness of "silceram" varied from 1.4 to 3.0 MPa.$m^{-1/2}$, bending strength from 90 to 262 MPa (depending on the production method), while potential applications of the material include thermal shock, erosion, impact and abrasion resistant components.

About 60 wt.% of blast furnace slag from China Baowu Iron & Steel Group (chemical composition of slag, in wt.%, 31.92 SiO_2, 15.12 Al_2O_3, 39.81 CaO, 8.54 MgO, 0.12 BaO, 0.39 Na_2O, 0.58 K_2O, 2.16 SO_3, 0.34 Fe_2O_3, 0.64 TiO_2 and 0.38 others) was applied in production GCs through conventional sintering method. To give an approximate indication of particular compositions, namely A1 and A4, the cross section of $CaO-MgO-SiO_2-Al_2O_3$ system with 10 and 15% of Al_2O_3 can be applied: both glass compositions A1 and A4 are positioned nearby pyroxene-melilite boundary (Table 3) and therefore precipitation of pertinent crystalline phases is anticipated. Actually, in the course of this investigation, gehlenite (to be more precise the binary solid solution gehlenite [$Ca_2Al_2SiO_7$] - akermanite [$Ca_2MgSi_2O_7$]) as the main phase and diopside along with hyalophane ($K_6Ba_4Al_{1.42}Si_{2.58}O_8$) were revealed after glass heat treatment at 890 °C for 1.5 h conferring to sintered glass A1 bulk density 2.77 g.cm^{-3}, bending strength 120.5 MPa and microhardness 610.21 HV [45].

Fly ash generated by the combustion process in thermal power plants and recovered by filtering operations is another industrial waste that was found even more convenient than blast furnace slag in GC production [46–48]. It is available in fine powder form and is basically composed of SiO_2, Al_2O_3, iron oxides, alkali- and alkaline-earth metal oxides plus several heavy metals and transition metal oxides. Carbon fly ash with glass cullet and float dolomite (coming from zinc extraction operations) were subjected to controlled crystallization in the 800°−1100 °C range [46]. Thus, the main precipitated crystalline phase in the experimental glass 4AP was pyroxene and the secondary feldspar anorthite owning to the fact that the pyroxene crystallization rate was higher than the feldspar rate. Approximate location of 4AP glass composition can be fixed either in the primary crystallization field of pyroxene within $CaO-MgO-SiO_2-Al_2O_3$ quaternary system with 15% Al_2O_3 or close to pyroxene-anorthite-forsterite join of the quaternary system with 20% Al_2O_3 (Table 3).

Fly ash-based glass sample with chemical composition (in wt.%) 43.35 SiO_2, 16.58 CaO, 5.92 MgO, 7.10 Fe_2O_3, 13.52 Al_2O_3, 5.12 Na_2O, 1.85 K_2O and 6.55 SO_3 was annealed for 10 h, nucleated at 687 °C for 5 h and crystallized at 892 °C for 20 min [47]. The XRD analysis confirmed that the main crystalline phase is diopside (*e.g.*, diopside solid solutions). This is consistent with an advanced anticipation since position of this composition in the phase diagram of $CaO-MgO-SiO_2-Al_2O_3$ system with 15% Al_2O_3 adjusted to the pyroxene primary field crystallization (Table 3).

Fly ash (FA) is a vastly produced waste in northern Greece thermal power stations of Ptolemaida that annually produce *ca.* 7 million tons of FA per year from the burning process of lignite coal. The chemical composition of this FA was (wt.%) 30.03 SiO_2, 13.67 Al_2O_3, 38.87 CaO, 5.32 Fe_2O_3, 4.42 MgO, 0.63 Na_2O, 0.59 K_2O, 6.17 SO_3, and 0.30 TiO_2. To produce glasses the batch composed of 52.78% fly ash, 24.96% silica, 2.68% alumina, and 19.58% magnesium carbonate was melted in alumina crucibles at 1500−1550 °C for 1 h in air [48]. The chemical compositions of the glasses studied in this work are adjusted to the primary crystallization field of pyroxene, in particular to the region neighbouring pyroxene-forsterite boundary in the phase diagram of $CaO-MgO-SiO_2-Al_2O_3$ system with 15% Al_2O_3 (Fig. 2, Table 3). Cr_2O_3, as nucleating agent, was applied in the amount of 0.50 wt.%, 0.75 wt.%, and 1.00 wt.%. Annealed glasses were subjected into two stage heat treatment in air: at 700 °C for 1 h for nucleation and then at different temperatures in the range of 900−1000 °C for 2 h for crystal growth. The highest value of bending strength 185 MPa was achieved after heat treatment at 900 °C when a single crystalline phase of augite

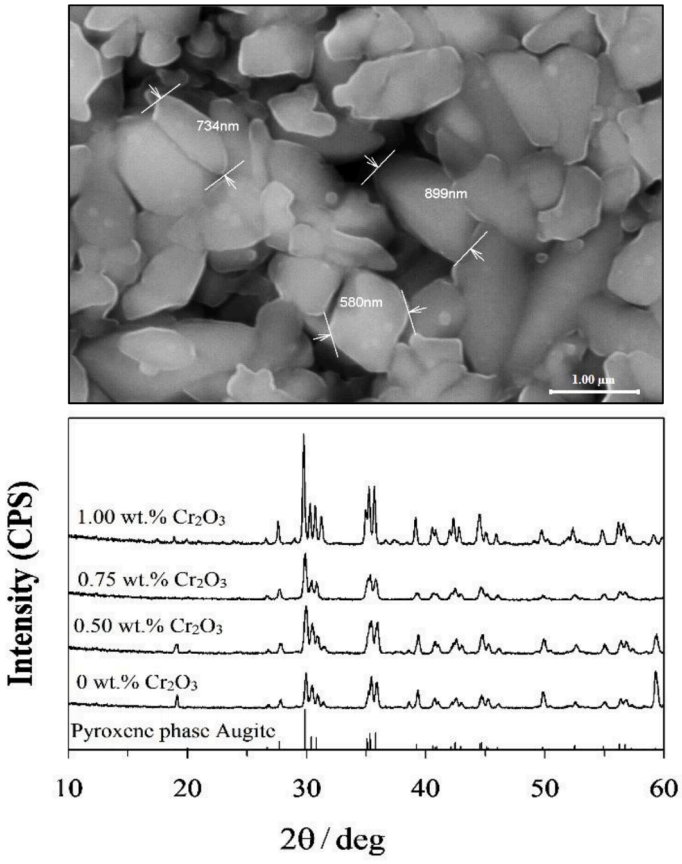

Fig. 3. X-ray diffractograms and typical SEM image of the investigated glass-ceramics crystallized at 900 °C for 2 h in air [48].

((Ca,Mg,Fe,Na)(Mg,Fe,Al,Ti)(Al,Si)$_2O_6$) was formed (Fig. 3). Fine grained bulk crystallized GCs was formed solely after adding nucleating agent, conversely, in Cr_2O_3-free GC crystallization initiated from the surface and resulted in structure that comprised coarse crystal layers sandwiched by residual glassy phase [48].

Waste generated from silica sand production was applied to glass-ceramics synthesis with diopside-anorthite crystalline phases. Position of the compositions studied on the liquidus surface of the cross section of $CaO-MgO-SiO_2-Al_2O_3$ system with 15% of Al_2O_3 neighbouring pyroxene-anorthite boundary (Sample 1) and pyroxene-anorthite-tridymite joint (Sample 2) [49]. After firing at 1000 °C diopside was the major and anorthite the secondary crystalline phase in the Sample 1 while in turn the opposite trend was in case of the Sample 2. Bending strength of the latter GC sample was 130 and of the former 73 MPa, suggesting that samples with diopside as the major crystalline phase possessed significantly higher mechanical strength.

Ball clay, dolomite and quartz sand were used as the main precursors to produce glass with composition 46.00 SiO_2, 23.50 CaO, 9.37 MgO, 1.20 Fe_2O_3, 15.90 Al_2O_3, 0.04 Na_2O, 0.98 K_2O, 0.42 TiO_2, 1.95 P_2O_5 and 0.35 CaF_2 (wt.%). This composition is located *ca* pyroxene-anorthite-akermanite joint on the liquidus surface of the cross section of $CaO-MgO-SiO_2-Al_2O_3$ system with 15% of Al_2O_3 (Table 4). Sintering of glass powder compacts at 920 °C resulted in GCs of akermanite-diopside-anorthite composition demonstrating bending strength of 112–113 MPa [50].

Compositions of iron-rich glasses produced using zinc hydrometallurgy waste, jarosite, granite mud and wastes from the cutting the blocks [42] are located in the elementary phase triangle diopside-protoenstatite-forsterite of the $CaO-MgO-SiO_2$ (Table 4, Fig. 1). Crystallization of glasses (Cr_2O_3 was added in the amount of 0.7%) at 800 °C confessed GCs with pyroxene as the major crystalline phase [42].

Basalts (cover about 70% of Earth surface) are promising precursors of GC technology [52]. Basalts are igneous rocks composed mainly of CaO, SiO_2, MgO, Al_2O_3 and iron oxides. According to the amount of SiO_2, appears as ultrabasic (SiO_2 <45%), basic (52%<SiO_2<45%), intermediate (66%<SiO_2) and acidic (SiO_2 >66%). Homogeneous bubble free glasses were produced at 1400–1450 °C from basaltic rock (composition, wt.%: 45.90 SiO_2, 16.55 Al_2O_3, 11.80 Fe_2O_3, 1.49 TiO_2, 10.85 CaO, 8.30 MgO, 3.24 Na_2O, 0.76 K_2O, 0.41 L.O.I.) that was used in the amount of 50–90% (the other material was ceramic waste). When analysing compositions containing 50 and 60% of basalt, they are located *ca* pyroxene-anorthite boundary in the quaternary system $CaO-MgO-SiO_2-Al_2O_3$ system with 20% Al_2O_3 (Table 4). This feature governs structure of crystallized glasses because augite and anorthite were revealed as the main crystalline phases after heat treatment at 1100 °C [51].

There is a constant search for new alternatives of abundant and an environment-friendly materials for glass making that do not harm the environment. In this regard finding the most fusible glass compositions that lie in the diopside crystallization field or in the neighbouring regions may undoubtedly translate into significant energy savings without compromising quality of the final product [53].

4. Recent advancement in synthesis of glasses and glass ceramics of $CaO-MgO-SiO_2$ system for application as sealants for SOFC

The ability of diopside accommodate various cations (Ba^{2+}, Sr^{2+}, La^{3+}, Cr^{3+}, Al^{3+}, B^{3+}, etc.), in conjunction with the possibility of achieving desired physical properties and high chemical durability, has generated a great interest application of GCs based on diopside structural units in fuel cells as a robust sealing material.

There are following crucial requirements for SOFC sealant: (a) the sealants must have a coefficient of thermal expansion (CTE) in general in the range of (9–13) × 10^{-6} K^{-1}; (b) good mechanical properties; (c) electrical resistance > 2 kΩ.cm, to avoid parallel currents; and (d) be chemically compatible with other fuel cell components, while minimizing thermal stresses during high-temperature operations [54,55].

Thus, GC seals with diopside ($Ca_{0.89}$ $Mg_{1.11}Si$ O_6), as the main crystalline phase and substantial amount of a residual amorphous phase, demonstrated very good interfacial compatibility with $Mn_{1.5}Co_{1.5}O_4$ coated Crofer22APU and YSZ. It was revealed that after 500 h of thermal cycling (RT–800 °C) in air atmosphere with no crack's formation, interactions, or failure were observed [56].

Appropriate thermal and chemical properties along with high stability demonstrated pyroxene based $CaO-MgO-SrO-BaO-La_2O_3-Al_2O_3-SiO_2$ seal GC compositions that have been specifically discussed elsewhere [13]. In this series of GCs, the initial seal compositions were designed after finding that up to 30 mol% Ca-Tschermak (CaTs: $CaAl_2SiO_6$) is soluble in Diopside (Di: $CaMgSi_2O_6$), while the properties achieved for the 80 mol% Di: 20 mol% CaTs glass composition ($CaMg_{0.8}Al_{0.4}Si_{1.8}O_6$) (Fig. 4) are near the required sealant properties range [57,58].

Further substitution via scheme 0.1 (Ca^{2+} + Si^{4+}) = 0.1 (La^{3+} + Al^{3+}) in stoichiometric diopside system was examined to get composition with molecular formulae $Ca_{0.9}MgAl_{0.1}La_{0.1}Si_{1.9}O_6$. This glass after heat treatment at 850 °C for 300 h in air formed a rather smooth interface in contact with Croffer 22 APU [59–61].

Subsequently, $Ca_{0.9}MgAl_{0.1}La_{0.1}Si_{1.9}O_6$ composition investigated in the previous studies, was chosen as the starting point and new glasses namely Di-Ba-1, Di-Ba-2 and Di-Ba-3 (Table 5) were produced by introducing different concentrations of barium disilicate ($BaSi_2O_5$) [62]. Diopside solid solution crystallized as the single phase in all the glasses

Table 4
Some compositions of diopside-containing GCs produced from natural raw materials such as rocks and other precursors. Note that some conventions were applied to anticipate approximate indication of glass composition on the liquids surface of the corresponding phase diagrams: MgO and Fe_2O_3 were integrated and then the content of the major constituents was recalculated to set 100% at the expense of the rest components.

Type of the waste	Parent glass composition, wt.%					Approximate glass composition in the phase diagram		Ref.
	SiO_2	CaO	MgO/ Fe_2O_3	Al_2O_3	The rest	$CaO–MgO–SiO_2–Al_2O_3$ (0/10%)	$CaO–MgO–SiO_2–Al_2O_3$ (15/20%)	
Waste from silica sand production - Sample 1	52.9	17.7	9.5/0.4	16.2	3.3	–	Pyroxene-anorthite boundary	[49]
Waste from silica sand production - Sample 2	60.4	17.9	5.3/0.5	17.9	4.3	–	Pyroxene-anorthite -tridymite join (quaternary system with 15% Al_2O_3)	
Ball clay, dolomite, quartz sand	46.0	23.5	9.4/1.2	15.9	4.3	–	Pyroxene-anorthite-akermanite join (quaternary system with 15% Al_2O_3)	[50]
Zinc Hydrometallurgy waste, jarosite, granite mud	50.0	11.6	0.3/ 24.8	3.8	9.5	Elementary phase triangle diopside-protoenstatite-forsterite (ternary system)	–	[42]
Basaltic rock at Harrat Hishb, ceramics wastes	55.6–58.0	6.2–7.2	10.7/ 12.5	18.0–18.4	5.4	–	Pyroxene-anorthite boundary (quaternary system with 20% Al_2O_3)	[51]

Fig. 4. Microstructure (after chemical etching of polished surfaces with HF solution) of the monomineral glass-ceramics in Di: CaTs series, heat treated 850 °C: augite crystals embedded in the glassy matrix.

Table 5
Nominal batch compositions of the glasses in diopside-barium disilicate ($BaSi_2O_5$).

Glass	CaO	MgO	BaO	Al_2O_3	La_2O_3	SiO_2	B_2O_3	NiO
Di-Ba-1								
wt%	21.09	16.84	1.36	2.13	6.81	48.77	2.00	1.00
mol%	22.14	24.60	0.52	1.23	1.23	47.79	1.69	0.79
Di-Ba-2								
wt%	20.55	16.41	2.72	2.08	6.63	48.61	2.00	1.00
mol%	21.77	24.19	1.05	1.21	1.21	48.06	1.71	0.80
Di-Ba-3								
wt%	19.47	15.55	5.44	1.97	6.28	48.29	2.00	1.00
mol%	21.01	23.34	2.15	1.17	1.17	48.62	1.74	0.81

after at 900 °C for 300 h suggesting a relatively good stability of phases upon prolonged isothermal heat treatment.

In general, the CTE of GC sintered at 900 °C for 1 h varied in the range (9.7-10.9) × 10^{-6} K^{-1} while after long heat treatment at 900 °C for 300 h it changed in the interval (9.7–10.6) × 10^{-6} K^{-1}. Density and bending strength at 900 °C for 1 h change in the interval 3.08–3.19 g. cm^{-3} and 164–184 MPa, respectively. All the GC seals bonded well to Crofer22APU metallic interconnect, no gaps were observed, and the investigated interfaces showed homogeneous microstructures over their entire cross-sections of the joint (Fig. 5).

The very promising glass composition Di-Ba-1 discussed in previous section was used as the starting point for synthesis another series of glasses and was developed by partial substitution Sr for Ca in the same composition aiming at (i) tailoring CTE of parent glass and crystallized material; (ii) improving the wetting behavior of the sealants via reducing viscosity of the glasses in the deformation temperature interval; and (ii) achieving stable thermo-mechanical properties of sintered glass-powder compacts. Sr replaced 10, 20, 30 and 40% of Ca in the $Ca_{0.9}MgAl_{0.1}La_{0.1}Si_{1.9}O_6$ component of the parent glass having the following composition, mol.%: 22.14 CaO, 24.60 MgO, 0.52 BaO, 1.23 Al_2O_3, 1.23 La_2O_3, 47.79 SiO_2, 1.69 B_2O_3, 0.79 NiO (Table 6). As result T_g decreased and coefficient of thermal expansion (CTE) increased by Sr for Ca substitution in pyroxene glasses. The CTE values for SrO-containing glasses varied in the interval (10.0–11.3) × 10^{-6} K^{-1}: the CTE significantly increased at first addition of SrO reaching the maximum when Sr replaced 20 and 30% of Ca with some decline at further SrO increment. Additionally, SrO-containing glasses exhibited a viscosity of ~10^6 dPa.s at 900 °C, which is suitable for joining of SOFC metallic/ceramic components by glass/GC sealing upon stack hermetization [63].

Diopside ($CaMgSi_2O_6$) solid solution crystallized as the only phase in the Sr-0 GCs whilst Sr-containing glasses exhibited a tendency to form Sr-containing diopside solid solution phases. Importantly, that no other impurity crystalline phases were developed in both Sr-free and Sr-containing glasses after prolonged heat treatment at 900 °C for 250, 500 and 1000 h (Fig. 6).

Sr-0.3 GC exhibited highest CTE (11.2 × 10^{-6} K^{-1}) among GCs sintered at 900 °C for 1 h. No significant changes in thermal expansion were observed in SrO-containing GCs after long heat treatment at 900 °C for 1000 h compared to the parent GCs (Table 7).

Regarding mechanical properties, Sr-0 GCs attained maximum bending strength values varied between 156 and 172 MPa whilst Sr-0.4 GCs demonstrate minimum values of 125–115 MPa (Table 7). However, compared to parent SrO-free GCs, SrO-containing compositions exhibited remarkable stability in retaining mechanical strength after prolonged heat treatments. The values of average flexural strengths for all the GCs are about 1.5–2.5 times higher than those reported for GC-9 glass (41–78 MPa) [64], H-sintered bar (55 MPa) and B-sintered bar (91 MPa) [63].

To minimize thermal stresses during cell operation the differences in CTEs between interconnect and the seal glass should not exceed, in general, 1 × 10^{-6} K^{-1}. All the studied SrO-containing GCs exhibited their CTE in the range (9.6–11.2) × 10^{-6} K^{-1} that are nearly equal to CTE of parent glasses (10–11.3) × 10^{-6} K^{-1}. Considering CTE values for metallic interconnect (Crofer22 APU; Sanergy HT) varying in the range (11–12) × 10^{-6} K^{-1}, and ceramic electrolyte (*i.e.*, 8YSZ) to be (10–12) × 10^{-6} K^{-1} both the parent glasses and corresponding GC composition Sr-0.2, Sr-0.3 and Sr-0.4 (Table 7) should be suitable for rigid glass/GC seals.

Fig. 7 shows the SEM image of the interfaces between Sanergy HT/glass–ceramic for Sr-0.3 glasses, along with the corresponding EDS mappings of the relevant elements existing at the interface after heat treatment at 900 °C for 1 h in air. Neither spinel nor a chromium oxide layer and any other interfacial reactions were detected at the interfaces by SEM/EDS analyses, within the limits of experimental uncertainty as was observed in case of SrO-containing glasses [65,66].

For all studied Sr-containing GCs, the Arrhenius dependencies of the total conductivity are linear (Fig. 8), confirming that no phase changes take place after sintering at 900 °C. All the sealants possess excellent insulating properties in the temperature range necessary for SOFC operation; their electrical resistivity is higher than 2 MOhm.cm [67,68].

From the studies performed on synthesis reliable diopside GCs composition Sr-0.3 GCs could be used as a rigid GC layer in a multilayer seal due to the following reasons: (i) good sintering ability suitable for SOFC sealants; (ii) stable phase assemblage with >85% crystallized fraction after 250 h of heat treatment, (iii) excellent thermal stability properties such as CTE and mechanical strength along a period of 1000 h at 900 °C, (iv) well bonding to the Sanergy HT metallic interconnect (v) the stability of electrical conductivity in various atmosphere during the period of 250 h and (vi) good thermal shock resistance with 8YSZ ceramic plate.

Summarizing the current data, it is worth to conclude that although significant progress has been achieved in development reliable diopside-based GC sealants their performance over a longer period under fuel cell working conditions requires more investigations. Additionally, Sr-containing seals are recommended as starting point to develop innovative self-healing GC layer fulfilling all the required properties [69].

5. Bioactive glasses and glass ceramics for biomedical application

Ceramics, GCs and bioglasses of CaO−MgO−SiO_2 system have showed high capacity of bio-reparation and bioactivity on bone tissue surface by HA formation [70–73]. In particular, bioactive glasses in the CaO–MgO–SiO_2 system, as a special type of bioceramics, are able to bond to bone and stimulate new bone growth, fact that make them ideal candidates for applications in tissue engineering domain.

Thus, it was demonstrated that glasses of the CaO−MgO−SiO_2

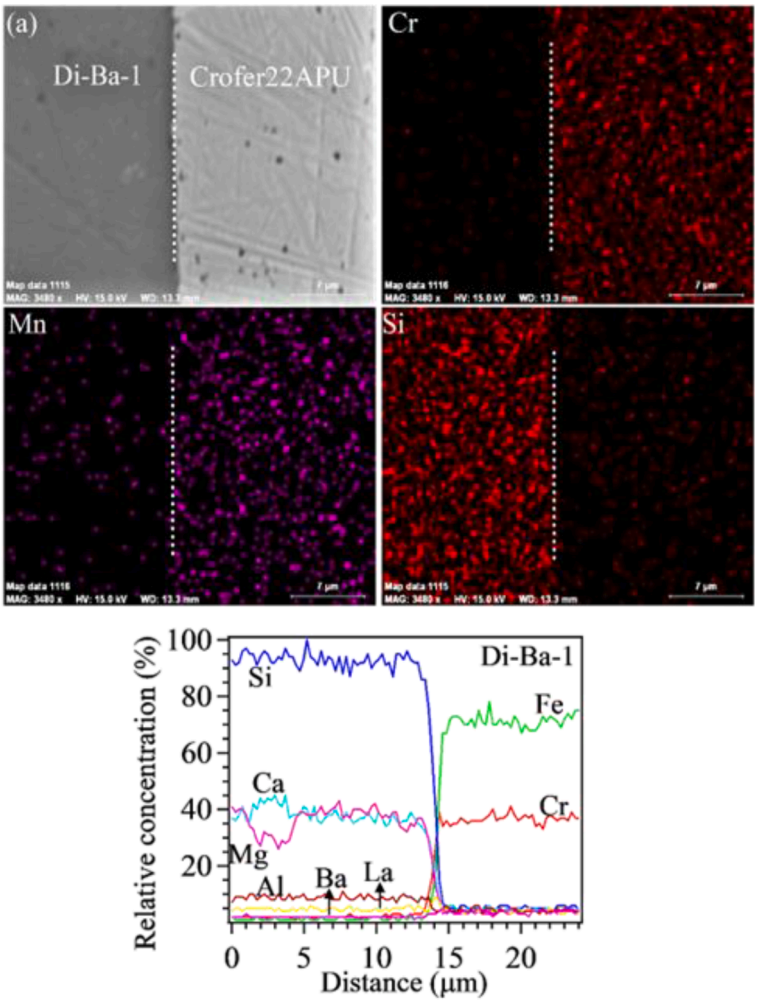

Fig. 5. Elemental distribution profiles for Cr, Fe, Si, Al, La, Ca and Mg elements along the interface of Di-Ba-1 GC/Crofer22APU (a).

Table 6
Chemical composition of SrO-containing glasses.

Glass	CaO	MgO	BaO	SrO	Al_2O_3	La_2O_3	SiO_2	B_2O_3	NiO
Sr-0.0									
Wt%	21.09	16.84	1.36	0.00	2.13	6.81	48.77	2.00	1.00
Mol%	22.14	24.60	0.52	0.00	1.23	1.23	47.79	1.69	0.79
Sr-0.1									
Wt%	18.36	16.5	1.36	4.24	2.09	6.67	47.79	2.00	1.00
Mol%	19.67	24.58	0.53	2.46	1.23	1.23	47.77	1.73	0.80
Sr-0.2									
Wt%	15.74	16.17	1.36	8.31	2.04	6.53	46.84	2.00	1.00
Mol%	17.19	24.56	0.54	4.91	1.23	1.23	47.75	1.76	0.82
Sr-0.3									
Wt%	13.23	15.85	1.36	12.22	2.00	6.40	45.94	2.00	1.00
Mol%	14.73	24.54	0.55	7.36	1.23	1.23	47.73	1.79	0.84
Sr-0.4									
Wt%	10.81	15.54	1.36	15.98	1.97	6.28	45.07	2.0	1.00
Mol%	12.26	24.52	0.56	9.81	1.23	1.23	47.71	1.83	0.85

system with B_2O_3, Na_2O, CaF_2, P_2O_5 additives favoured the formation of the A-type HA with increase in the P_2O_5 amount [74]. The proportions between the major constituents (*i.e.*, CaO, MgO and SiO_2) were set to be close the composition in the invariant equilibrium of the eutectic type 35.6 wt.% CaO, 12.8 wt.% MgO and 51.6 wt.% SiO_2, liquid ⇆ wollastonite + diopside + akermanite [75]. The boron free glasses from this series exhibited higher rates of bioactivity *in vitro* and osteoblast proliferation in cell culture medium with no evidence of any toxicity or other detrimental effects in the functionality of cells [76]. Further, bioactive glass BG1d-BG (composition in wt.%: 46.1 SiO_2, 28.7 CaO, 8.8 MgO, 6.2 P_2O_5, 5.7 CaF_2, 4.5 Na_2O) was proved to be biocompatible not only upon implantation into rabbit femurs, but also when used clinically for the treatment of jawbone defects [77,78]. Additionally, BG1d-BG possessed an advantage in regard to cell viability and proliferation of human mesenchymal stem cells (MSCs) compared to the 45S5 Bioglass due to combined effect of the lower amount of Na ions and the presence of Mg ions [79].

Knowing that the presence of MgO promotes formation of HA,

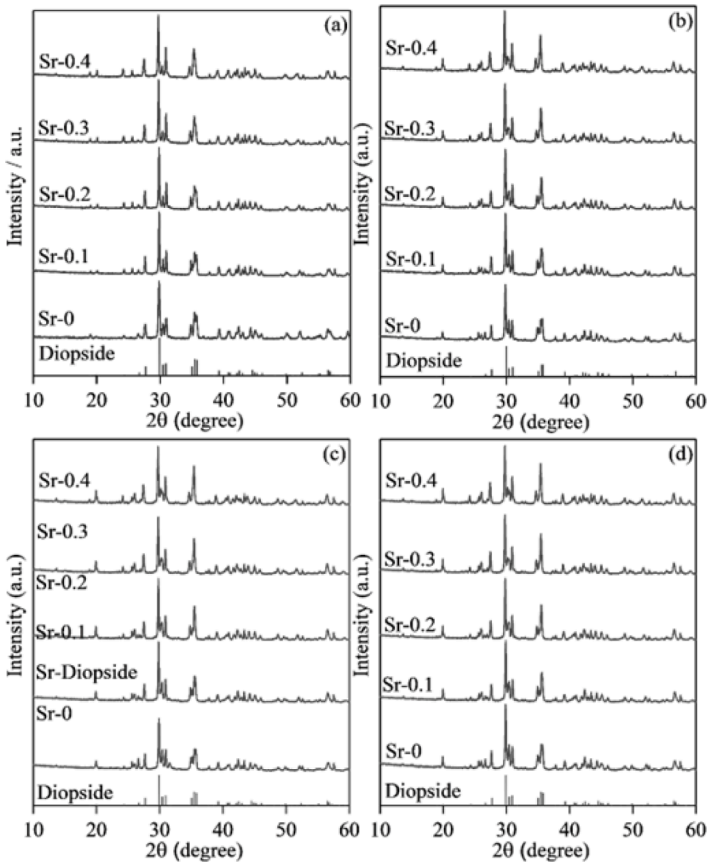

Fig. 6. XRD pattern of glass–ceramics sintered at 900 °C for: (a) 1 h; (b) 250 h; (c) 500 h; and (d) 1000 h.

Table 7
Bending strength (MPa) and CTE (±0.1) × 10^{-6} K^{-1} (200–700 °C) data measured for the glass-powder compacts after sintering at 900 °C for 1 h, 250 h, 500 h and 1000 h.

Composition	1 h	250 h	500 h	1000 h
Bending Strength				
Sr-0	172±4	162±7	161±9	156±8
Sr-0.1	160±5	158±4	154±1	150±4
Sr-0.2	150±7	141±3	150±7	144±5
Sr-0.3	137±7	125±3	133±5	133±8
Sr-0.4	125±3	123±4	122±3	115±3
CTE				
Sr-0	10.4	9.2	10.4	9.60
Sr-0.1	10.8	10.6	10.0	10.1
Sr-0.2	10.2	10.8	9.8	10.8
Sr-0.3	11.2	9.9	10.0	10.4
Sr-0.4	10.3	10.5	10.4	10.7

increases cell adhesion, proliferation and differentiation of osteoblast cells, new Mg-containing bioactive silicate glasses were studied for applications in cementum/alveolar bone regeneration [80]. These glasses are suggested for synthesis of scaffolds for hard tissue regeneration as they present a high residual glassy phase, acceptable hardness values (1.36 GPa, close to the corresponding values of cortical and trabecular bone, Table 8), hydroxyapatite-forming ability after 10 days of immersion in SBF, and high cell viability since cultured cells are homogenously distributed over the whole surface of the struts. Other research groups have also studied the effect of MgO on physical and mechanical properties of bioactive glasses in the CaO−MgO−SiO_2 system. Thus, after MgO addition Young's modulus bulk annealed glasses increased from 80.89 to 81.57 GPa [81] whilst the partial substitution of MgO for CaO led to bioactive glasses, with values of microhardness ~4.95−5.1 GPa, and positive machinability value n, which anticipates their capacity for being produced in any desired shape and tailored for each patient via milling techniques [82].

The structure of bioactive glasses designed in diopside ($CaO{\cdot}MgO{\cdot}2SiO_2$)-tricalcium phosphate ($3CaO{\cdot}P_2O_5$) system according to NMR spectra is composed of network consisting mostly of Q^2 and Q^3 (Si) units, whose proportion depends on diopside content. The produced glasses displayed bioactivity performance after 7 days of soaking in SBF and a significant statistical increase in metabolic activity of human mesenchymal stem cells was observed for Di-60 and Di-70 glass compositions under both basal and osteogenic conditions [83].

Actually, the phase diagram of diopside-fluorapatite system that features eutectic point at 1250 °C with 77.5 wt.% $CaMgSi_2O_6$ and 22.5 wt.% $Ca_5(PO_4)_3F$ and S-shaped liquidus curve in the range of 30 wt.% and 60 wt.% fluorapatite (*e.g.*, evidencing occurrence of liquid-liquid phase separation) [22] inaugurated series of alkali-free bioactive glass compositions [84–88]. Further, a promising HA forming ability in biological liquids was revealed for bioactive glass compositions of ternary $CaMgSi_2O_6$ (Di) - $Ca_5(PO_4)_3F$ (FA) - $Ca_3(PO_4)_2$ (TCP) system especially for 70Di–10FA–20TCP composition that was designated as FastOs®BG [89]. Investigation of osteogenic activity and histological assessments of samples tested in a sheep animal model demonstrated that FastOs®BG is more slowly resorbed, more biocompatible and osteoconductive, and more easily osteointegrated in comparison to 45S5 Bioglass®. Thus, it was proposed that FastOs®BG could possess greater potential as a bone graft material for large bone defects [90]. The foremost information on processing methods, structural features and properties of FastOs®BG and its derivatives as well as another alkali-free bioactive glass is provided elsewhere [91].

Referring again to the phase diagram of diopside-fluorapatite system it is worth to mention that glass compositions located near the binary eutectic after crystallization demonstrated high rate of apatite-forming

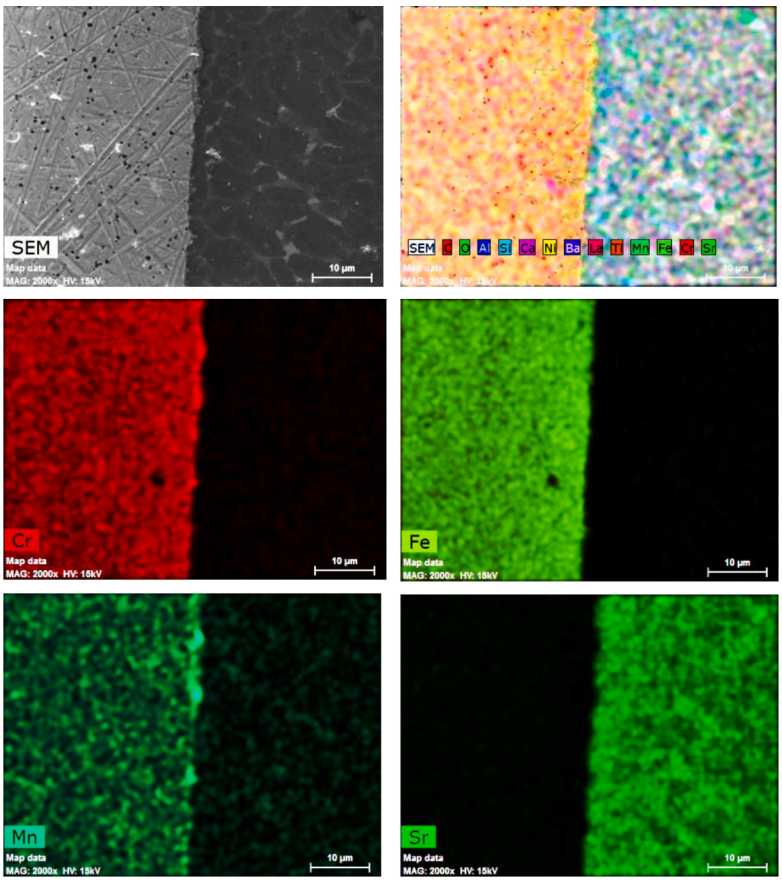

Fig. 7. SEM image and EDS element mappings for Cr, Fe, Mn and Sr at the interface between Sr-0.3 and Sanergy HT after heat treatment at 900 °C for 1 h.

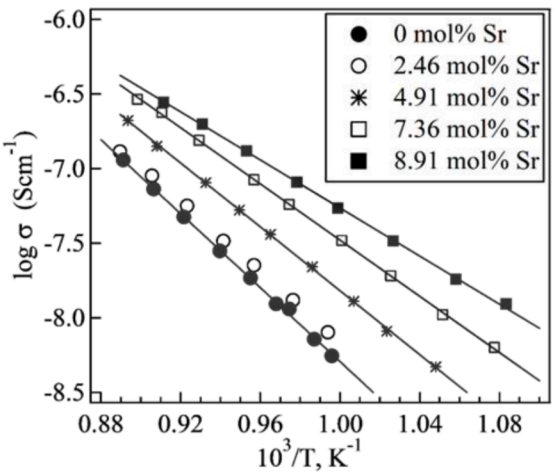

Fig. 8. Temperature dependencies of the total electrical conductivity in atmospheric air.

ability on their surfaces upon *in vitro* SBF testing with good biodegradation properties Additionally, *in vitro* responses of MSCs to these GCs showed favourable growth behaviours suggesting GCs as potential materials for tissue engineering [23,25].

In the other similar work [26] evaluated crystallization in tetrasilicic mica (TSM, $KMg_{2.5}Si_4O_{10}F_2$) - fluorapatite (FA, $Ca_5(PO_4)_3F$) - diopside (Di, $CaMgSi_2O_6$) system, the microstructure of the investigated annealed glasses clearly featured liquid-liquid phase separation: phase separation enhanced with apatite and diopside addition causing nucleation within the droplet glass phases. For instance, the microstructure of glass 25.0% TSM, 37.5% FA and 37.5% D (composition in wt%: 35.46 SiO_2, 28.48 CaO, 10.66 MgO, 15.83 P_2O_5, 2.9 CaF_2, 3.8 MgF_2, 2.87 K_2O) is presented by spheres/ellipsoids with average dimensions of 0.4−0.5 μm embedded in glass matrix (Fig. 9,a). This glass featured high capability for bulk crystallization with mica, apatite and diopside over heating between 700 and 1075 °C and demonstrated unusual whiskers like HA crystals formation on their surface upon soaking in SBF solution (Fig. 9,b).

Recently, CaO−MgO−SiO_2 GCs in a specific molar ratio of 1:1:2 to meet the molar ratio of diopside phase were synthesized with 8.5 wt.% ZrO_2 additive as a nucleation agent to modulate the ratios between the glass and GC phases as a function of sintering temperature [10]. According to authors ZrO_2 was selected because the addition of this oxide from 3.0 to 8.5 wt.% confesses the stabilization of diopside crystalline phase formation and increases the strain and toughness of the produced material. The formation of diopside crystalline phase in the investigated GCs initiated at 820 °C and facilitates with further increase in sintering temperature. The developed GCs possessed the highest flexural strength of ~190 MPa and compressive strength of ~555 MPa when sintered at 850–900 °C and 850 °C, respectively. As can be seen in Table 8, these values are very close to the corresponding values of cortical bone. Apparently, both flexural strength and compressive strength can be tuned according to the proportion between diopside and amorphous glassy phase. GCs display biocompatibility, and osteoconductivity: more specifically, an *in-vivo* experiment demonstrated a fine bone-ingrowth profile around the GC implant that was grafted onto the femurs of rats for three months. The above results demonstrated an opportunity for using the investigated GCs in bone implants and artificial intervertebral discs. It is important to note that the addition of ZrO_2 did not negatively affect the biological behavior of the material, and at the same time allows the adjustment of mechanical properties based on the ratios of crystalline and amorphous phases.

Table 8
Comparison of mechanical properties of the presented Diopside containing GCs [10,92,93,95-98] with the corresponding values of the human natural tissues [92,99].

Reference	Flexural strength (MPa)	Modulus of elasticity (GPa)	Compressive strength (MPa)	Micro-hardness (GPa)	Fracture toughness ($MPa.m^{0.5}$)	Proposed application
Properties of natural tissues						
HA [99]	60–120	–	100–150	0.09–0.14	$0.8^{-1}.2$	–
Dentine [98]	230–305	15–30		< 0.6 GPa	3	–
Cortical bone [98]	50–150	7–30	100–135	0.06–0.075	$2^{-1}2$	–
Trabecular bone [98]	10–20	0.05–0.5	1.5–7.5	0.5^{-1}	$0.7^{-1}.1$	–
Diopside GCs and proposed biomedical applications						
[10]	~60–190	–	~ 467–555	–	–	Bone implants Artificial intervertebral discs
[98]	120–177	27–34	–	6.0–6.7	2.1–2.6	Dental Implants
[93]	120–195	–	–	–	–	Biomedical applications (generally)
[95]	–	–	0.83–1.46	–	–	Scaffolds for bone repair
[96]	–	–	0.05–0.8	–	–	Scaffolds for bone repair
[97]	–	1.4	29.7	–	–	Scaffolds for bone repair

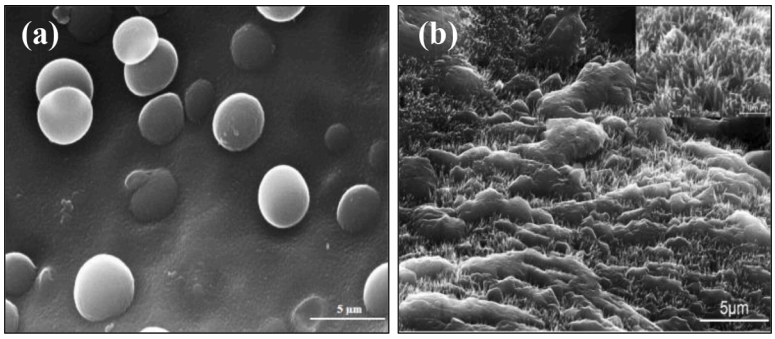

Fig. 9. SEM images of the (a) as cast glass of 25.0% TSM, 37.5% FA, 37.5% D and (b) bulk GCs of the same composition after exposition in SBF solution.

Although the addition of Al_2O_3 to bioactive glasses improves the long-term stability of implants needed for bone defect repair and increases the mechanical properties of GCs, unlike ZrO_2 the addition of Al_2O_3 significantly compromises the bioactivity of the materials. It was generally accepted that up to 1.5 wt.% Al_2O_3 can be accommodated by the glass structure without significantly reducing the bioactivity. Aiming at getting more insights on this matter and to improve mechanical properties of GCs 1 mol% (~1.7 wt.%) Al_2O_3 was added to bioactive GCs in the CaO−MgO−SiO_2 ternary system [92]. As a result, dense and well-sintered GCs composed of diopside, wollastonite, and fluorapatite crystalline phases were produced by sintering of glass-powder compacts. Indeed, the addition of 1 mol% (~ 1.7 wt.%) Al_2O_3 improved the mechanical properties of the resultant materials: GCs featured modulus of elasticity 27–34 GPa, microhardness 6.0–6.7 GPa, and fracture toughness 2.1–2.6 $MPa.m^{0.5}$, which are in a good match to those of human jawbone and dentine (Table 8). Moreover, the developed GCs were potentially bioactive, which was witnessed by the formation of HA on their surface after their immersion in SBF [92].

Well sintered and mechanically strong (flexural strength 120−195 MPa is very close to the corresponding values of cortical bone, Table 8) GCs with diopside as major crystalline were obtained via crystallization alkali-free bioactive glasses with partial replacement of MgO by ZnO (2, 4, 6, 8, and 10 mol%). After immersion samples in SBF, ZnO content was found to play an essential role on the *in vitro* bioactivity. The GC composition with ZnO = 4 mol% exhibited the highest levels of mesenchymal cell proliferation and alkaline phosphatase activity, while further increasing ZnO contents led to a significant decrease in the *in vitro* performance of the investigated GCs. According to the results, although ZnO has been shown to have an important role in bioactivity, and cell proliferation and alkaline phosphatase activity, but the addition of this oxide must be carefully studied before the final design of the composition [93].

Compositions based on a CaO−MgO−SiO_2 system obtained from silicon-based mixtures and Ca/Mg-rich glass have been investigated as candidate materials for biomedical applications. According to XRD results the specimens were crystallized, mainly forming wollastonite and diopside Also, among the composition studied, the wollastonite/diopside GCs heat-treated at 1100 °C (WD2–1100) showed good bioactivity and no cytotoxicity, and the evidence from this work suggests that WD2–1100 GCs may be successfully used as a bone defect filler in the tissue engineering domain [94].

In recent years, several attempts have been made to fabricate porous ceramic materials with controlled porous structures. Thus, using freeze-drying technique for the manufacture of HA porous scaffolds which were coated with diopside (impregnated in the diopside sol before gel formation for 1, 2, and 5 days) and then sintered to prepare diopside/HA composite scaffolds, studied the bioactivity, degradation behavior and physico-mechanical properties of the prepared scaffolds were obtained [95]. Bioactivity performance of diopside/HA scaffolds was detected through the genesis of an HA layer over the surface and their acceptable degradation rate in comparison to that of the blank HA scaffold. According to authors the amount of diopside that diffused within the HA scaffolds during the coating process influenced both the porosity and compressive strength values. Regarding mechanical strength of the diopside/HA scaffolds the compressive strength increased from 0.83 ± 0.06 (1 day) to 1.46 ± 0.05 MPa (5 days). Another research team [96] studied the presence of diopside crystalline phase in porous GCs in the CaO−MgO−SiO_2 ternary system. More specifically, porous GCs containing β-TCP (β) and diopside (Di) crystalline phases in proportion 60β/40Di, 50β/50Di, 38β/62Di and 100Di were synthesized. In agreement with experimental results the higher compressive strength values was recorded for GC 38β/62Di (0.8 MPa) and followed 100Di (~0.35 MPa), 50β/50Di (~0.1 MPa), 60β/40Di (~0.05 MPa). This porous GCs, with continuous pores of about 500 μm, revealed bioactivity

performance after immersion of specimens in SBF for 3 (60β/40Di, 50β/50Di), 7 (38β/62Di) and 14 (100Di) days. These GCs are expected to be useful as scaffold materials for bone repair (trabecular bone).

Porous GCc scaffolds were produced by foam replication using aforementioned BG-1d BG glass. Upon high-temperature thermal treatment, the glass underwent sinter-crystallization, leading to consolidation of the scaffold structure and concurrent development of three biocompatible crystalline phases, *i.e.*, diopside, fluorapatite, and wollastonite. The scaffolds exhibited a 3D pore–strut architecture and total porosity (68 vol%) matching those of spongy bone, while the compressive strength (29.7 MPa) and elastic modulus (1.4 GPa) were superior to those of osseous tissue, suggesting suitability for application in load-bearing sites. The scaffolds also exhibited highly promising bioactive properties *in vitro*, being covered by a calcium phosphate layer after immersion in simulated body fluids for just 48 h [97].

By comparing the values of the compressive strength of the aforementioned porous GCs [95–97] with the corresponding values of cortical and trabecular bone (Table 8), the developed GC materials could be used as candidate filling materials to replace trabecular bone in places that are not subjected to intense loading [95,96] or GC materials for application in load-bearing sites [97].

Biomaterials aim to replace damaged or lost parts or functions of the human body in a safe, reliable, and nature-compatible manner (and certainly at low cost), to restore the original function of the human body. This means that an ideal biomaterial must have properties as close as possible to those of the tissue that the biomaterial is intended to replace, and thus must have a good relationship with the tissues that were directly adjacent to the lost tissue, as Mother Nature wisely intended for all body tissues. Based on the above, one of the aims of this brief review was to compare the values of mechanical properties of the diopside-containing GCs [10,92,93,95–97] with the corresponding values of the hard tissues such as HA, dentine, trabecular and cortical bone (Table 8). Summarizing the current data it is worth to conclude that although the diopside GCs are competitive materials for biomedical applications due to their bioactivity and biocompatibility (no cytotoxicity) and some attractive mechanical properties (Table 8), it would be important to conduct additional experimental trials to synthesize materials with mechanical properties resemble properties of natural bone, as these materials are being studied as candidates for biomedical applications such as orthopaedics and dentistry, where the materials are subjected to dynamically changing loads.

6. Some other active areas of research and application for diopside containing glass-ceramic compositions

As may be apparent from the discussion thus far, the special attention the current review was drawn to diopside containing compositions appropriate for application as sealants in solid oxide fuel cells and as competitive materials for biomedical applications. Surely $CaO-MgO-SiO_2$ glasses and GCs are increasingly the subject of materials research towards novel high functional applications. To give an example, the diopside GC was demonstrated to possess enhanced microwave dielectric properties, excellent chemical durability as well as appropriate mechanical properties at low sintering temperature being suitable candidate for low temperature co-fired ceramics LTCC technology [100–107]. In this context, considerable efforts have been made to investigate the role of nucleating agents and sintering aids on sinter-crystallization behavior of GCs and their correlation with microwave dielectric characteristics. Thus, when glass of stoichiometric diopside composition was prepared utilizing conventional melt quenching technique, the corresponding GC of diopside exhibited high-Q microwave dielectric of 56,952 GHz and 64,524 GHz, depending on sintering parameters of the initial glass [102]. Other diopside GCs with a TiO_2 content of 5–20 wt.% were prepared by a by a sinter-crystallization technique [103]. Dielectric constant demonstrated tendency to rise while the quality factor to decline with increase in TiO_2 content that was attributed to the formation of notable quantities of titanite as the secondary phase with a high dielectric constant of about 45 at a frequency of 1 MHz. The highest relative density (about 99%) and dielectric constant 8.8–9.5 were obtained for the GCs sintered at 800 °C for 4 h which was due to minimal crystallinity. The role of another nucleating agent Cr_2O_3 on various properties of GCs with diopside as the main crystalline phase was evaluated as well. The results showed that the sample containing 0.7 wt.% Cr_2O_3 possessed the best dielectric and mechanical properties [104].

It is worth mentioning that diopside-based GC has been studied from the very beginning for nuclear waste immobilization [108–110] with the aim of producing pyroxene by remelting natural basalt rock together with calcined waste oxides. Nowadays, immobilization of high-level nuclear wastes by developing GC waste forms that have high chemical durability in the natural environment and high tolerance to radiation damage continues to be an active research area for environmental and safety reasons [110–113].

Additionally, GCs with augite as a major crystalline phase was produced for immobilizing lanthanide-containing mining wastes owning to possibility of La for Ca substitution in the clinopyroxene structure [114]. Likewise, GCs based on diopside was recommended for immobilization of heavy metals Pb and Cd from incinerator waste [115].

7. Conclusions

Glasses and GCs in the $CaO-MgO-SiO_2$ system are one of the most promising among the various silicate systems because of the abundance of reagents, simpler fabrication, improved performance, and wide range of applications. This brief review shows that glasses and diopside-containing GC can be used in a wide range of applications, *i.e.*, from innovative sealants for SOFC to biomaterials for bone repair.

The most fusible eutectic in the $CaO-MgO-SiO_2$ system is formed between wollastonite, diopside and tridymite with a melting point of 1320 °C. The diopside crystallization field is limited by two more eutectics with the lowest melting points: one between diopside, akermanite and wollastonite - 1350 °C, the second between diopside, akermanite and forsterite - 1357 °C. Apparently, the most fusible compositions lie in the diopside crystallization field or in the neighbouring regions. The crystallization paths of melts in the $CaO-MgO-SiO_2$ system is often complex and is affected by metastable segregation and formation of pyroxene solid solutions. In this regard, the selection of the most fusible glass compositions may undoubtedly translate into significant energy savings without compromising quality of the final product.

SiO_2, Al_2O_3, iron oxides, alkali- and alkaline-earth metal oxides are the main constituents of vastly produced wastes such as blast furnace slags and fly ashes and naturally occurring basaltic rocks. To anticipate formation of crystalline phases and to guide GC production from wastes, basalts, new alternatives of abundant and an environment-friendly materials cross sections of $CaO-MgO-SiO_2-Al_2O_3$ system with 10, 15, 20 and 25% of Al_2O_3 are more appropriate to apply instead of $CaO-MgO-SiO_2$.

Due to the ability of diopside to accommodate various cations (Ba^{2+}, Sr^{2+}, La^{3+}, Cr^{3+}, Al^{3+}, B^{3+}, etc.), in conjunction with the possibility of achieving desired physical properties and high chemical durability, series of glasses and GCs have been synthesized, thoroughly characterized and proposed for application as robust sealing material for SOFC. Diopside-based SrO–containing GCs exhibited their CTE in the range (9.6–11.2) $\times 10^{-6}$ K^{-1} that are nearly equal to CTE for metallic interconnect (Crofer22 APU; Sanergy HT) varying in the range (11–12) $\times 10^{-6}$ K^{-1}, and ceramic electrolyte (*i.e.*, 8YSZ) to be (10–12) $\times 10^{-6}$ K^{-1}. Their remarkable stability in retaining mechanical strength after prolonged heat treatments, excellent insulating properties and high thermal shock resistance recommend them to be used as a rigid GC layer in a multilayer seal for SOFCs and other high temperature electrochemical devices.

Bioactive glasses in the $CaO–MgO–SiO_2$ system, as a special type of

bioceramics, are able to bond to bone and stimulate new bone growth, which make them ideal material for applications in tissue engineering domain. In particular, the advantages of alkali-free or low alkali-containing bioactive glass compositions from CaO–MgO–SiO_2 system in regard to cell viability and proliferation of human mesenchymal stem cells (MSCs) when compared to the 45S5 Bioglass opens new frontiers for their advancement in healthcare domain.

Diopside-containing GCs are promising materials for biomedical applications because they combine bioactivity, no cytotoxicity, and mechanical strength in the same material. This fact highlights these materials as competitive candidates among other ceramic materials for biomedical applications in dentistry, orthopaedics and scaffolds fabrication for bone regeneration where the materials are subjected to dynamically changing loads.

Declaration of Competing Interest

The authors declare that they have no known competing financial interests or personal relationships that could have appeared to influence the work reported in this paper.

Data availability

Data will be made available on request.

Acknowledgments

HRF thank CICECO-Aveiro Institute of Materials, UIDB/50011/2020, UIDP/50011/2020 & LA/P/0006/2020, financed by national funds through the FCT/MCTES (PIDDAC).

References

[1] V.R. Mastelaro, P.S. Bayer, E.D. Zanotto, Crystallization mechanism and kinetics of a Fe-diopside (25CaO·25MgO·50SiO_2) glass–ceramic, J. Mater. Sci. 54 (2019) 9313–9320, https://doi.org/10.1007/s10853-019-03572-y.

[2] N. Karpukhina, R.G. Hill, R.V. Law, Crystallisation in oxide glasses - a tutorial review, Chem. Soc. Rev. 43 (2014) 2174–2186, https://doi.org/10.1039/c3cs60305a.

[3] A.M. Segadaes, Use of phase diagrams to guide ceramic production from wastes, Adv. Appl. Ceram. 105 (2006) 46–54, https://doi.org/10.1179/174329006X82927.

[4] C. Fredericci, E.D. Zanotto, E.C. Ziemath, Crystallization mechanism and properties of a blast furnace slag glass, J. Non. Cryst. Solids 273 (2000) 64–75, https://doi.org/10.1016/S0022-3093(00)00145-9.

[5] C. Lira, A.P.N. de Oliveira, O.E. Alarcon, Sintering and crystallisation of CaO-Al_2O_3-SiO_2 glass powder compacts, Glass Technol. 42 (2001) 91–96.

[6] I.H. Jung, S.A. Decterov, A.D. Pelton, Critical thermodynamic evaluation and optimization of the CaO-MgO-SiO_2 system, J. Eur. Ceram. Soc. 25 (2005) 313–333, https://doi.org/10.1016/j.jeurceramsoc.2004.02.012.

[7] W. Höland, G.H. Beall, Glass Ceramic Technology, 2nd ed., John Wiley & Sons, Inc., Hoboken, 2012 https://doi.org/10.1002/9781118265987.

[8] X. Chen, X. Liao, Z. Huang, P. You, C. Chen, Y. Kang, G. Yin, Synthesis and characterization of novel multiphase bioactive glass-ceramics in the CaO-MgO-SiO_2 system, J. Biomed. Mater. Res. B Appl. Biomater. 93B (2010) 194–202, https://doi.org/10.1002/jbm.b.31574.

[9] M. Zhang, X. Pu, X. Chen, G. Yin, In-vivo performance of plasma-sprayed CaO–MgO–SiO_2-based bioactive glass-ceramic coating on Ti–6Al–4V alloy for bone regeneration, Heliyon 5 (2019), e02824, https://doi.org/10.1016/j.heliyon.2019.e02824.

[10] K.C. Feng, Y.J. Wu, C.Y. Wang, C.S. Tu, Y.L. Lin, C.S. Chen, P.L. Lai, Y.T. Huang, P.Y. Chen, Enhanced mechanical and biological performances of CaO-MgO-SiO2 glass-ceramics via the modulation of glass and ceramic phases, Mater. Sci. Eng. C 124 (2021), 112060, https://doi.org/10.1016/j.msec.2021.112060.

[11] C. Wu, J. Chang, A review of bioactive silicate ceramics, Biomed. Mater. 8 (2013) 032001, doi:10.1088/1748-6041/8/3/032001.

[12] C. Saravanan, S. Sasikumar, Bioactive diopside ($CaMgSi_2O_6$) as a drug delivery carrier - A review, Curr. Drug Deliv. 9 (2012) 583–587, https://doi.org/10.2174/156720112803529765.

[13] D.U. Tulyaganov, A.A. Reddy, V.V. Kharton, J.M.F. Ferreira, Aluminosilicate-based sealants for SOFCs and other electrochemical applications - A brief review, J. Power Sources 242 (2013) 486–502, https://doi.org/10.1016/j.jpowsour.2013.05.099.

[14] M.K. Mahapatra, K. Lu, Seal glass for solid oxide fuel cells, J. Power Sources 195 (2010) 7129–7139, https://doi.org/10.1016/j.jpowsour.2010.06.003.

[15] J.W. Fergus, Sealants for solid oxide fuel cells, J. Power Sources 147 (2005) 46–57, https://doi.org/10.1016/j.jpowsour.2005.05.002.

[16] R. Spotorno, M. Ostrowska, S. Delsante, U. Dahlmann, P. Piccardo, Characterization of glass-ceramic sealant for solid oxide fuel cells at operating conditions by electrochemical impedance spectroscopy, Materials (Basel) 13 (2020) 1–13, https://doi.org/10.3390/ma13214702.

[17] J. Ferguson, H. Merwin, The ternary system CaO-MgO-SiO_2, Proc. Natl. Acad. Sci. U. S. A. 5 (1919) 16–18, https://doi.org/10.1073/pnas.5.1.16.

[18] E.F. Osborn, A. Muan, Phase equilibria diagrams of oxide systems. American Ceramic Society, Columbus, 1960.

[19] M.M. Smedskjaer, M. Jensen, Y.-Z. Yue, Theoretical calculation and measurement of the hardness of diopside, J. Am. Ceram. Soc. 91 (2008) 514–518, https://doi.org/10.1111/j.1551-2916.2007.02166.x.

[20] M.L.F. Nascimento, E.B. Ferreira, E.D. Zanotto, Kinetics and mechanisms of crystal growth and diffusion in a glass-forming liquid, J. Chem. Phys. 121 (2004) 8924–8928, https://doi.org/10.1063/1.1803813.

[21] S. Reinsch, M.L.F. Nascimento, R. Müller, E.D. Zanotto, Crystal growth kinetics in cordierite and diopside glasses in wide temperature ranges, J. Non. Cryst. Solids 354 (2008) 5386–5394, https://doi.org/10.1016/j.jnoncrysol.2008.09.007.

[22] D.U. Tulyaganov, Phase equilibrium in the fluorapatite-anorthite-diopside system, J. Am. Ceram. Soc. 83 (2000) 2141–3146, https://doi.org/10.1111/j.1151-2916.2000.tb01695.x.

[23] R. Conradt, On the entropy difference between the vitreous and the crystalline state, J. Non. Cryst. Solids 355 (2009) 636–641, https://doi.org/10.1016/j.jnoncrysol.2008.12.013.

[24] F.L. Galeener, D.L. Griscom, M.J. Weber. Defects in Glasses, Materials Research, Society, Pittsburgh, 1986.

[25] E.D. Zanotto, Surface nucleation in a diopside glass, J. Non. Cryst. Solids 130 (1991) 217–219, https://doi.org/10.1016/0022-3093(91)90458-I.

[26] L. Wondraczek, H. Behrens, Y. Yue, J. Deubener, G.W. Scherer, Relaxation and glass transition in an isostatically compressed diopside glass, J. Am. Ceram. Soc. 90 (2007) 1556–1561, https://doi.org/10.1111/j.1551-2916.2007.01566.x.

[27] S. Kroeker, J.F. Stebbins, Magnesium coordination environments in glasses and minerals: new insight from high-field magnesium-25 MAS NMR, Am. Mineral. 85 (2000) 1459–1464, https://doi.org/10.2138/am-2000-1015.

[28] J. Schneider, V.R. Mastelaro, H. Panepucci, E.D. Zanotto, ^{29}Si MAS-NMR studies of Q^n structural units in metasilicate glasses and their nucleating ability, J. Non. Cryst. Solids 273 (2000) 8–18.

[29] J.B. Murdoch, J.F. Stebbins, I.S.E. Carmichael, High-resolution ^{29}Si NMR study of silicate and aluminosilicate glasses; the effect of network-modifying cations, Am. Mineral. 70 (1985) 332–343.

[30] A.B. Corradi, F. Bondioli, V. Cannillo, A.M. Ferrari, I. Lancellotti, M. Montorsi, The anorthite-diopside system: structural and devitrification study. Part I: structural characterization by molecular dynamic simulations, J. Am. Ceram. Soc. 88 (2005) 714–718, https://doi.org/10.1111/j.1551-2916.2005.00142.x.

[31] Y. Yue, The iso-structural viscosity, configurational entropy and fragility of oxide liquids, J. Non. Cryst. Solids 355 (2009) 737–744, https://doi.org/10.1016/j.jnoncrysol.2009.01.032.

[32] H. Taniguchi, T. Murase, Some physical properties and melt structures in the system diopside-anorthite, J. Volcanol. Geotherm. Res. 34 (1987) 51–64, https://doi.org/10.1016/0377-0273(87)90092-8.

[33] H. Taniguchi, Entropy dependence of viscosity and the glass-transition temperature of melts in the system diopside-anorthite, Contrib. Mineral. Petrol. 109 (1992) 295–303, https://doi.org/10.1007/BF00283319.

[34] C.M. Scarfe, D.J. Cronin, J.T. Wenzel, D.A. Kauffman, Viscosity-temperature relationships at 1 atm in the system diopside-anorthite, Am. Mineral. 68 (1983) 1083–1088.

[35] P. Tauber, J. Arndt, The relationship between viscosity and temperature in the system anorthite-diopside, Chem. Geol. 62 (1987) 71–81, https://doi.org/10.1016/0009-2541(87)90058-1.

[36] T.B. King, The surface tension and structure of silicate slags, J. Soc. Glass Technol. 35 (1951) 241–259.

[37] H. Taniguchi, Surface tension of melts in the system $CaMgSi_2O_6$-$CaAl_2Si_2O_8$ and its structural significance, Contrib. Mineral. Petrol. 100 (1988) 484–489, https://doi.org/10.1007/BF00371377.

[38] P. Alizadeh, V.K. Marghussian, Study of bulk crystallization in MgO-CaO-SiO_2-Na_2O glasses in the presence of CaF_2 and MoO_3 nucleant, J. Mater. Sci. 38 (2003) 1529–1534, https://doi.org/10.1023/A:1022984918108.

[39] S.A.M. Abdel-Hameed, A.A. El-kheshen, Thermal and chemical properties of diopside-wollastonite glass-ceramics in the SiO_2-CaO-MgO system from raw materials, Ceram. Int. 29 (2003) 265–269, https://doi.org/10.1016/S0272-8842(02)00114-1.

[40] A. Karamanov, I. Penkov, B. Bogdanov, Diopside marble-like sintered glass-ceramics, Glastechn. Ber. 67 (1994) 202–206.

[41] L.R. Pinckney, in: Glass ceramics, encyclopedia of materials: Science and Technology, Pergamon, Oxford, 2001, https://doi.org/10.1016/b0-08-043152-6/00629-x.

[42] A. Karamanov, P. Pisciella, M. Pelino, The effect of Cr_2O_3 as a nucleating agent in iron-rich glass-ceramics, J. Eur. Ceram. Soc. 19 (1999) 2641–2645, https://doi.org/10.1016/s0955-2219(99)00047-3.

[43] R.D. Rawlings, J.P. Wu, A.R. Boccaccini, Glass-ceramics: their production from wastes - A review, J. Mater. Sci. 41 (2006) 733–761, https://doi.org/10.1007/s10853-006-6554-3.

[44] D.U. Tulyaganov, S. Agathopoulos, V.V. Kharton, F.M.B. Marques, Glass-ceramics in the former Soviet Union: a review on industry-oriented developments, Ind. Ceram. 23 (2003) 101–116.

[45] L.I. Zuhao, H.E. Feng, W. Zhang, X.I.E. Junlin, Structure and properties of glass-ceramics from blast furnace slag with different Al_2O_3/SiO_2 ratio, Ceram. Silikaty 65 (2021) 187–197, https://doi.org/10.13168/cs.2021.0018.

[46] L. Barbieri, I. Lancellotti, T. Manfredini, G.C. Pellacani, J.M. Rincòn, M. Romero, Nucleation and crystallization of new glasses from fly ash originating from thermal power plants, J. Am. Ceram. Soc. 84 (2001) 1851–1858, https://doi.org/10.1111/j.1151-2916.2001.tb00926.x.

[47] M. Erol, S. Küçükbayrak, A. Ersoy-Meriçboyu, M.L. Öveçollu, Crystallization behaviour of glasses produced from fly ash, J. Eur. Ceram. Soc. 21 (2001) 2835–2841, https://doi.org/10.1016/S0955-2219(01)00221-7.

[48] K.C. Vasilopoulos, D.U. Tulyaganov, S. Agathopoulos, M.A. Karakassides, J.M. F. Ferreira, D. Tsipas, Bulk nucleated fine grained mono-mineral glass-ceramics from low-silica fly ash, Ceram. Int. 35 (2009) 555–558, https://doi.org/10.1016/j.ceramint.2008.01.002.

[49] T. Toya, Y. Tamura, Y. Kameshima, K. Okada, Preparation and properties of CaO-MgO-Al_2O_3-SiO_2 glass-ceramics from kaolin clay refining waste (Kira) and dolomite, Ceram. Int. 30 (2004) 983–989, https://doi.org/10.1016/j.ceramint.2003.11.005.

[50] D.U. Tulyaganov, M.J. Ribeiro, J.A. Labrincha, Development of glass-ceramics by sintering and crystallization of fine powders of calcium-magnesium-aluminosilicate glass, Ceram. Int. 28 (2002) 515–520, https://doi.org/10.1016/S0272-8842(02)00004-4.

[51] G.A. Khater, A. Abdel-Motelib, A.W. El Manawi, M.O. Abu Safiah, Glass-ceramics materials from basaltic rocks and some industrial waste, J. Non. Cryst. Solids 358 (2012) 1128–1134, https://doi.org/10.1016/j.jnoncrysol.2012.02.010.

[52] L.F. de Lima, J.E. Zorzi, R.C.D. Cruz, Basaltic glass-ceramic: a short review, Bol. Soc. Esp. Ceram. Vidr. 61 (2022) 2–12, https://doi.org/10.1016/j.bsecv.2020.07.005.

[53] J. Feng, D. Wu, M. Long, K. Lei, Y. Sun, X. Zhao, Diopside glass-ceramics were fabricated by sintering the powder mixtures of waste glass and kaolin, Ceram. Int. 48 (2022) 27088–27096, https://doi.org/10.1016/j.ceramint.2022.06.020.

[54] L.D. Silva, A.M. Rodrigues, A.C.M. Rodrigues, M.J. Pascual, A. Durán, A. A. Cabral, Sintering and crystallization of SrO-CaO-B_2O_3-SiO_2 glass-ceramics with different TiO_2 contents, J. Non. Cryst. Solids 473 (2017) 33–40, https://doi.org/10.1016/j.jnoncrysol.2017.07.021.

[55] M.J. Pascual, V.V. Kharton, E. Tsipis, A.A. Yaremchenko, C. Lara, A. Durán, J. R. Frade, Transport properties of sealants for high-temperature electrochemical applications: RO-BaO-SiO_2 (R = Mg, Zn) glass-ceramics, J. Eur. Ceram. Soc. 26 (2006) 3315–3324, https://doi.org/10.1016/j.jeurceramsoc.2005.11.002.

[56] F. Smeacetto, A. De Miranda, A. Chrysanthou, E. Bernardo, M. Secco, M. Bindi, M. Salvo, A.G. Sabato, M. Ferraris, Novel glass-ceramic composition as sealant for SOFCs, J. Am. Ceram. Soc. 97 (2014) 3835–3842, https://doi.org/10.1111/jace.13219.

[57] A. Goel, D.U. Tulyaganov, S. Agathopoulos, M.J. Ribeiro, R.N. Basu, J.M. F. Ferreira, Diopside-Ca-Tschermak clinopyroxene based glass-ceramics processed via sintering and crystallization of glass powder compacts, J. Eur. Ceram. Soc. 27 (2007) 2325–2331, https://doi.org/10.1016/j.jeurceramsoc.2006.07.016.

[58] A. Goel, D.U. Tulyaganov, S. Agathopoulos, M.J. Ribeiro, J.M.F. Ferreira, Crystallization behaviour, structure and properties of sintered glasses in the diopside-Ca-Tschermak system, J. Eur. Ceram. Soc. 27 (2007) 3231–3238, https://doi.org/10.1016/j.jeurceramsoc.2007.01.018.

[59] A. Goel, D.U. Tulyaganov, V.V. Kharton, A.A. Yaremchenko, S. Eriksson, J.M. F. Ferreira, Optimization of La_2O_3-containing diopside based glass-ceramic sealants for fuel cell applications, J. Power Sources 189 (2009) 1032–1043, https://doi.org/10.1016/j.jpowsour.2009.01.013.

[60] A. Goel, D.U. Tulyaganov, A.M. Ferrari, E.R. Shaaban, A. Prange, F. Bondioli, J.M. F. Ferreira, Structure, sintering process and crystallization kinetics of alkaline-earth aluminosilicate glasses suitable for SOFC, J. Am. Ceram. Soc. 93 (2010) 830–837, https://doi.org/10.1111/j.1551-2916.2009.03503.x.

[61] A. Goel, D.U. Tulyaganov, M.J. Pascual, E.R. Shaaban, F. Muñoz, Z. Lü, J.M. F. Ferreira, Development and performance of diopside based glass-ceramic sealants for solid oxide fuel cells, J. Non. Cryst. Solids 356 (2010) 1070–1080, https://doi.org/10.1016/j.jnoncrysol.2010.01.012.

[62] A.A. Reddy, D.U. Tulyaganov, A. Goel, M.J. Pascual, V.V. Kharton, E.V. Tsipis, J. M.F. Ferreira, Diopside - Mg orthosilicate and diopside - Ba disilicate glass-ceramics for sealing applications in SOFC: sintering and chemical interactions studies, Int. J. Hydrogen Energy 37 (2012) 12528–12539, https://doi.org/10.1016/j.ijhydene.2012.05.130.

[63] A.A. Reddy, D.U. Tulyaganov, M.J. Pascual, V.V. Kharton, E.V. Tsipis, V. A. Kolotygin, J.M.F. Ferreira, Diopside-Ba disilicate glass-ceramic sealants for SOFCs: enhanced adhesion and thermal stability by Sr for Ca substitution, Int. J. Hydrogen Energy 38 (2013) 3073–3086, https://doi.org/10.1016/j.ijhydene.2012.12.074.

[64] H.T. Chang, C.K. Lin, C.K. Liu, High-temperature mechanical properties of a glass sealant for solid oxide fuel cell, J. Power Sources 189 (2009) 1093–1099, https://doi.org/10.1016/j.jpowsour.2008.12.102.

[65] I.W. Donald, P.M. Mallinson, B.L. Metcalfe, L.A. Gerrard, J.A. Fernie, Recent developments in the preparation, characterization and applications of glass- and glass-ceramic-to-metal seals and coatings, J. Mater. Sci. 46 (2011) 1975–2000, https://doi.org/10.1007/s10853-010-5095-y.

[66] T. Zhang, Q. Zou, F. Zeng, S. Wang, D. Tang, H. Yang, Improving the chemical compatibility of sealing glass for solid oxide fuel cells: blocking the reactive species by controlled crystallization, J. Power Sources 216 (2012) 1–4, https://doi.org/10.1016/j.jpowsour.2012.05.034.

[67] A.A. Reddy, D.U. Tulyaganov, M.J. Pascual, V.V. Kharton, E.V. Tsipis, V. A. Kolotygin, J.M.F. Ferreira, SrO-containing diopside glass-ceramic sealants for solid oxide fuel cells: mechanical reliability and thermal shock resistance, Fuel Cells 13 (2013) 689–694, https://doi.org/10.1002/fuce.201200237.

[68] A.A. Reddy, D.U. Tulyaganov, G.C. Mather, M.J. Pascual, V.V. Kharton, S. I. Bredikhin, V.A. Kolotygin, J.M.F. Ferreira, Effect of strontium-to-calcium ratio on the structure, crystallization behavior and functional properties of diopside-based glasses, Int. J. Hydrogen Energy 39 (2014) 3552–3563, https://doi.org/10.1016/j.ijhydene.2013.12.104.

[69] A.A. Reddy, N. Eghtesadi, D.U. Tulyaganov, M.J. Pascual, L.F. Santos, S. Rajesh, F.M.B. Marques, J.M.F. Ferreira, Bi-layer glass-ceramic sealant for solid oxide fuel cells, J. Eur. Ceram. Soc. 34 (2014) 1449–1455, https://doi.org/10.1016/j.jeurceramsoc.2013.11.012.

[70] Z. Strnad, Role of the glass phase in bioactive glass-ceramics, Biomaterials 13 (1992) 317–321, https://doi.org/10.1016/0142-9612(92)90056-T.

[71] P.N. De Aza, Z.B. Luklinska, M. Anseau, Bioactivity of diopside ceramic in human parotid saliva, J. Biomed. Mater. Res. B Appl. Biomater. 73B (2005) 54–60, https://doi.org/10.1002/jbm.b.30187.

[72] N.Y. Iwata, G.H. Lee, Y. Tokuoka, N. Kawashima, Sintering behavior and apatite formation of diopside prepared by coprecipitation process, Colloids Surfaces B Biointerfaces 34 (2004) 239–245, https://doi.org/10.1016/j.colsurfb.2004.01.007.

[73] T. Nonami, S. Tsutsumi, Study of diopside ceramics for biomaterials, J. Mater. Sci. Mater. Med. 10 (1999) 475–479. http://www.ncbi.nlm.nih.gov/pubmed/15348115.

[74] S. Agathopoulos, D.U. Tulyaganov, J.M.G. Ventura, S. Kannan, M. A. Karakassides, J.M.F. Ferreira, Formation of hydroxyapatite onto glasses of the CaO–MgO–SiO_2 system with B_2O_3, Na_2O, CaF_2 and P_2O_5 additives, Biomaterials 27 (2006) 1832–1840, https://doi.org/10.1016/j.biomaterials.2005.10.033.

[75] D.U. Tulyaganov, S. Agathopoulos, J.M. Ventura, M.A. Karakassides, O. Fabrichnaya, J.M.F. Ferreira, Synthesis of glass-ceramics in the CaO-MgO-SiO_2 system with B_2O_3, P_2O_5, Na_2O and CaF_2 additives, J. Eur. Ceram. Soc. 26 (2006) 1463–1471, https://doi.org/10.1016/j.jeurceramsoc.2005.02.009.

[76] D.U. Tulyaganov, S. Agathopoulos, P. Valerio, A. Balamurugan, A. Saranti, M. A. Karakassides, J.M.F. Ferreira, Synthesis, bioactivity and preliminary biocompatibility studies of glasses in the system CaO–MgO–SiO_2–Na_2O–P_2O_5–CaF_2, J. Mater. Sci. Mater. Med. 22 (2011) 217–227, https://doi.org/10.1007/s10856-010-4203-5.

[77] D.U. Tulyaganov, M.E. Makhkamov, A. Urazbaev, A. Goel, J.M.F. Ferreira, Synthesis, processing and characterization of a bioactive glass composition for bone regeneration, Ceram. Int. 39 (2013) 2519–2526, https://doi.org/10.1016/j.ceramint.2012.09.011.

[78] D.U. Tulyaganov, F. Baino, Silicate glasses and glass-ceramics: types, role of composition and processing methods, in: Ceramics, Glass and Glass-Ceramics,, Springer, 2021, https://doi.org/10.1007/978-3-030-85776-9_4.

[79] S.I. Schmitz, B. Widholz, C. Essers, M. Becker, D.U. Tulyaganov, A. Moghaddam, F. Juan, I. Gonzalo de Westhauser, Superior biocompatibility and comparable osteoinductive properties: sodium-reduced fluoride-containing bioactive glass belonging to the CaO-MgO-SiO_2 system as a promising alternative to 45S5 bioactive glass, Bioact. Mater. 5 (2020) 55–65, https://doi.org/10.1016/j.bioactmat.2019.12.005.

[80] O.M. Goudouri, E. Kontonasaki, K. Chrissafis, K. Zinn, A. Hoppe, R. Detsch, K. M. Paraskevopoulos, A.R. Boccaccini, Towards the synthesis of an Mg-containing silicate glass-ceramic to be used as a scaffold for cementum/alveolar bone regeneration, Ceram. Int. 40 (2014) 16287–16298, https://doi.org/10.1016/j.ceramint.2014.07.066.

[81] E.A. Mahdy, Z.Y. Khattari, W.M. Salem, S. Ibrahim, Study the structural, physical, and optical properties of CaO–MgO–SiO_2–CaF_2 bioactive glasses with Na_2O and P_2O_5 dopants, Mater. Chem. Phys. 286 (2022), 126231, https://doi.org/10.1016/j.matchemphys.2022.126231.

[82] K. Dimitriadis, D.U. Tulyaganov, K.C. Vasilopoulos, M.A. Karakassides, S. Agathopoulos, Influence of K and Mg substitutions on the synthesis and the properties of CaO-MgO-SiO_2/Na_2O, P_2O_5, CaF_2 bioactive glasses, J. Non. Cryst. Solids 573 (2021), 121140, https://doi.org/10.1016/j.jnoncrysol.2021.121140.

[83] S. Kapoor, Â. Semitela, A. Goel, Y. Xiang, J. Du, A.H. Lourenço, D.M. Sousa, P. L. Granja, J.M.F. Ferreira, Understanding the composition–structure–bioactivity relationships in diopside ($CaO.MgO.2SiO_2$)–tricalcium phosphate ($3CaO.P_2O_5$) glass system, Acta Biomater. 15 (2015) 210–226, https://doi.org/10.1016/j.actbio.2015.01.001.

[84] I. Kansal, D.U. Tulyaganov, A. Goel, M.J. Pascual, J.M.F. Ferreira, Structural analysis and thermal behavior of diopside-fluorapatite-wollastonite-based glasses and glass-ceramics, Acta Biomater. 6 (2010) 4380–4388, https://doi.org/10.1016/j.actbio.2010.05.019.

[85] I. Kansal, A. Goel, D.U. Tulyaganov, R. Raman, J.M.F. Ferreira, Structural and thermal characterization of CaO–MgO–SiO_2–P_2O_5–CaF_2 glasses, J. Eur. Ceram. Soc. 32 (2012) 2739–2746, https://doi.org/10.1016/j.jeurceramsoc.2011.10.041.

[86] I. Kansal, A. Goel, D.U. Tulyaganov, L.F. Santos, J.M.F. Ferreira, Structure, surface reactivity and physico-chemical degradation of fluoride containing phospho-silicate glasses, J. Mater. Chem. 21 (2011) 8074–8084, https://doi.org/10.1039/c1jm10811e.

[87] A. Goel, S. Kapoor, R.R. Rajagopal, M.J. Pascual, H.W. Kim, J.M.F. Ferreira, Alkali-free bioactive glasses for bone tissue engineering: a preliminary investigation, Acta Biomater. 8 (2012) 361–372, https://doi.org/10.1016/j.actbio.2011.08.026.

[88] S. Kapoor, A. Goel, M.J. Pascual, J.M.F. Ferreira, Alkali-free bioactive diopside–tricalcium phosphate glass-ceramics for scaffold fabrication: sintering and crystallization behaviours, J. Non. Cryst. Solids 432 (2016) 81–89, https://doi.org/10.1016/j.jnoncrysol.2015.05.033.
[89] J.M.F. Ferreira, A. Goel, Alkali-free bioactive glass composition, US Patent US 9238044 B2, US 9238044 B2, 2016.
[90] P.P. Cortez, A.F. Brito, S. Kapoor, A.F. Correia, L.M. Atayde, P. Dias-Prereira, A. C. Maurício, A. Afonso, A. Goel, J.M.F. Ferreira, The in vivo performance of an alkali-free bioactive glass for bone grafting, FastOs BG, assessed with an ovine model, J. Biomed. Mater. Res. B 105B (2017) 30–38, https://doi.org/10.1002/jbm.b.33529.
[91] H.R. Fernandes, A. Gaddam, A. Rebelo, D. Brazete, G.E. Stan, J.M.F. Ferreira, Bioactive glasses and glass-ceramics for healthcare applications in bone regeneration and tissue engineering, Materials (Basel) 11 (2018) 1–54, https://doi.org/10.3390/ma11122530.
[92] K. Dimitriadis, D. Moschovas, D.U. Tulyaganov, S. Agathopoulos, Development of novel bioactive glass-ceramics in the Na_2O/K_2O-CaO-MgO-SiO_2-P_2O_5-CaF_2 system, J. Non. Cryst. Solids 533 (2020), 119936, https://doi.org/10.1016/j.jnoncrysol.2020.119936.
[93] S. Kapoor, A. Goel, A. Filipa, M.J. Pascual, H. Lee, H. Kim, J.M.F. Ferreira, Influence of ZnO/MgO substitution on sintering, crystallisation, and bio-activity of alkali-free glass-ceramics, Mater. Sci. Eng. C 53 (2015) 252–261, https://doi.org/10.1016/j.msec.2015.04.023.
[94] A.D.C. Juraski, A.C.D. Rodas, H. Elsayed, E. Bernardo, V.O. Soares, J. Daguano, The in vitro bioactivity, degradation, and cytotoxicity of polymer-derived wollastonite-diopside glass-ceramics, Materials (Basel) 10 (2017) 425, https://doi.org/10.3390/ma10040425.
[95] M. Sayed, E.M. Mahmoud, F. Bondioli, S.M. Naga, Developing porous diopside/hydroxyapatite bio-composite scaffolds via a combination of freeze-drying and coating process, Ceram. Int. 45 (2019) 9025–9031, https://doi.org/10.1016/j.ceramint.2019.01.236.
[96] M. Kamitakahara, C. Ohtsuki, Y. Kozaka, S.I. Ogata, M. Tanihara, T. Miyazaki, Preparation of porous glass-ceramics containing whitlockite and diopside for bone repair, J. Ceram. Soc. Jpn. 114 (2006) 82–85, https://doi.org/10.2109/jcersj.114.82.
[97] F. Baino, D.U. Tulyaganov, Z. Kahharov, A. Rahdar, E. Verné, Foam-replicated diopside/fluorapatite/wollastonite-based glass–ceramic scaffolds, Ceramics 5 (2022) 120–130, https://doi.org/10.3390/ceramics5010011.
[98] K. Dimitriadis, D.U. Tulyaganov, S. Agathopoulos, Development of novel alumina-containing bioactive glass-ceramics in the CaO-MgO-SiO_2 system as candidates for dental implant applications, J. Eur. Ceram. Soc. 41 (2021) 929–940, https://doi.org/10.1016/j.jeurceramsoc.2020.08.005.
[99] G. Kaur, V. Kumar, F. Baino, J.C. Mauro, G. Pickrell, I. Evans, O. Bretcanu, Mechanical properties of bioactive glasses, ceramics, glass-ceramics and composites: state-of-the-art review and future challenges, Mater. Sci. Eng. C 104 (2019), 109895, https://doi.org/10.1016/j.msec.2019.109895.
[100] M.W. Chang, S.H. Lyoo, H.S. Choo, J.M. Lee, Properties of glasses based on the CaO-MgO-SiO_2 system for low-temperature co-fired ceramic, Ceram. Int. 35 (2009) 2513–2515, https://doi.org/10.1016/j.ceramint.2008.12.013.
[101] J.K. Christie, R.I. Ainsworth, N.H. De Leeuw, Investigating structural features which control the dissolution of bioactive phosphate glasses: beyond the network connectivity, J. Non. Cryst. Solids 432 (2016) 31–34, https://doi.org/10.1016/j.jnoncrysol.2015.01.016.
[102] M.K. Zitani, T. Ebadzadeh, S. Banijamali, R. Riahifar, C. Rüssel, S.K. Abkenar, H. Ren, High quality factor microwave dielectric diopside glass-ceramics for the low temperature co-fired ceramic (LTCC) applications, J. Non. Cryst. Solids 487 (2018) 65–71, https://doi.org/10.1016/j.jnoncrysol.2018.02.025.
[103] M. Kiani Zitani, S. Banijamali, C. Rüssel, S. Khabbaz Abkenar, P. Mokhtari, H. Ren, T. Ebadzadeh, Concurrent sinter-crystallization and microwave dielectric characterization of CaO-MgO-TiO_2-SiO_2 glass-ceramics, J. Asian Ceram. Soc. 8 (2020) 234–244, https://doi.org/10.1080/21870764.2020.1725258.
[104] Y. Han, X. Jia, F. Liu, L. Deng, X. Zhang, Effect of Cr_2O_3 content on high-temperature dielectric properties and crystallisation of CMAS glass-ceramics, Mater. Res. Express 6 (2019) 075213, doi:10.1088/2053-1591/ab180b.
[105] R. Huang, J. Pan, A.R. Boccaccini, Q.Z. Chen, A two-scale model for simultaneous sintering and crystallization of glass-ceramic scaffolds for tissue engineering, Acta Biomater. 4 (2008) 1095–1103, https://doi.org/10.1016/j.actbio.2008.02.004.
[106] G.A. Khater, B.S. Nabawy, J. Kang, M.A. Mahmoud, Dielectric properties of basaltic glass and glass-ceramics: modeling and applications as insulators and semiconductors, Silicon 11 (2019) 579–592.
[107] F. Kamutzki, S. Schneider, J. Barowski, A. Gurlo, D.A.H. Hanaor, Silicate dielectric ceramics for millimetre wave applications, J. Eur. Ceram. Soc. 41 (2021) 3879–3894, https://doi.org/10.1016/j.jeurceramsoc.2021.02.048.
[108] W. Lutze, R.C. Ewing. Radioactive Waste Forms For the Future, North-Holland Publishers, Amsterdam, 1988.
[109] S. Martinez, P. Alfonso, C. de la Fuente, I. Queralt. Glass ceramic materials from Spanish basalts, Centro de Investigaciones Energeticas Medioambientales y Tecnologicas (CIEMAT), and Instituto de Ceramica y Vidrio, Madrid, 1987.
[110] J.S. Mccloy, S. Schuller, Vitrification of wastes: from unwanted to controlled crystallization, a review, C. R. Géosci. 354 (2022) 121–160.
[111] I.W. Donald. The Science and Technology of Inorganic Glasses and Glass-Ceramics: From the Ancient to the Present to the Future, Society of Glass Technology, Shefield, 2016.
[112] N.C. Hyatt, M.I. Ojovan, Special issue: materials for nuclear waste immobilization, Materials (Basel) 12 (2019) 12–15, https://doi.org/10.3390/ma12213611.
[113] J.S. McCloy, A. Goel, Glass-ceramics for nuclear-waste immobilization, MRS Bull. 42 (2017) 233–240.
[114] H. Chen, B. Li, M. Zhao, X. Zhang, Y. Du, Y. Shi, J.S. McCloy, Lanthanum modification of crystalline phases and residual glass in augite glass ceramics produced with industrial solid wastes, J. Non. Cryst. Solids 524 (2019), 119638, https://doi.org/10.1016/j.jnoncrysol.2019.119638.
[115] K. Krausova, L. Gautron, A. Karnis, G. Catillon, S. Borensztajn, Glass ceramics and mineral materials for the immobilization of lead and cadmium, Ceram. Int. 42 (2016) 8779–8788, https://doi.org/10.1016/j.ceramint.2016.02.119.